

Journal of the Mechanics and Physics of Solids
Stochastic Calibration of Biological Tissue Biomechanics: Bridging In-Vitro
Measurements and In-Silico Simulations
--Manuscript Draft--

Manuscript Number:	MPS-D-25-00494R1
Article Type:	Full Length Article
Keywords:	In-vitro measurements, in-silico simulations, biological materials, uncertainty quantification, stochastic material calibration, approximate Bayesian computation, finite element method
Corresponding Author:	Mahmut Pekedis, PhD Ege University Izmir, TURKEY
First Author:	Mahmut Pekedis, PhD
Order of Authors:	Mahmut Pekedis, PhD
Abstract:	This study proposes a simple and practical approach based on in-vitro measurements and in-silico simulations using the likelihood-free Bayesian inference with the finite element method simultaneously for stochastic calibration and uncertainty quantification of the mechanical response of biological materials. We implement the approach for distal, middle, and proximal human Achilles tendon specimens obtained from diabetic patients post-amputation. A wide range of in-vitro loading conditions are considered, including one-step and two-step relaxation, as well as incremental cyclic loading tests. In-silico simulations are performed for the tendons assuming a fiber-reinforced viscoelastic response, which is modeled separately for the ground matrix and fiber components. Initially, the calibration of the specimen-specific parameters is predicted using Bayesian optimization and the sensitivity of each parameter is evaluated using the Sobol index and random forest. Then, the bounds of these parameters are used as priors, uniformly sampled, and coupled with in-vitro data in simulation-based approximate Bayesian computations to calibrate and quantify the uncertainty parameters for three loading cases. The results demonstrate that increasing the number of loading scenarios improves the accuracy of the specimen-specific best-fit parameter set. Furthermore, approximate Bayesian inference shows that in-silico simulations using the posterior parameters, can capture the uncertainty bounds of in-vitro measurements. This approach provides a useful framework for stochastic calibration of constitutive material model parameters without the need to derive a likelihood function, regardless of the specimen's geometry or loading conditions.

Dear Associate Editor Professor Ellen Kuhl,

We greatly appreciate your evaluation of our manuscript entitled "Stochastic Calibration of Biological Tissue Biomechanics: Bridging In-Vitro Measurements and In-Silico Simulations" submitted to the Journal of the Mechanics and Physics of Solids. We revised our manuscript in accordance with the Reviewers' insightful comments and suggestions. The changes in the revised manuscript are highlighted in red for clarity. Below, we provide point-by-point responses to each reviewer comment.

Kind Regards,

Reviewer #1

The paper discusses an interesting problem of model parameter estimation using Bayesian methods. It is well written and formatted. Some remarks and questions to improve the manuscript.

• We sincerely thank the Reviewer for the constructive comments, suggestions, and feedback, which significantly improved the manuscript. We revised the manuscript accordingly. All textual changes are highlighted in red.

(1) General: Punctuation marks are missing after equations that finish a sentence, e.g. 4, 13, ..

• We thank the Reviewer for pointing this out. We have carefully reviewed all equations in the manuscript and added appropriate punctuation marks (e.g., periods) after equations that conclude a sentence, including those referred to in the comment (e.g., Equations 4 and 13). This correction has been applied throughout the manuscript to ensure consistency with academic writing standards.

Below, we include the corrected versions of Equations 4 and 13.

Lines 125-127: The coefficients ξ and B are defined to ensure continuity of the strain energy function:

$$\xi = \frac{E_f(I_0 - 1)^{2-\beta} \exp[-\alpha(I_0 - 1)^\beta]}{4I_0^{3/2}(\beta - 1 + \alpha\beta(I_0 - 1)^\beta)},$$
$$B = E_f \frac{2I_0(\beta - \frac{1}{2} + \alpha\beta(I_0 - 1)^\beta) - 1}{4I_0^{3/2}(\beta - 1 + \alpha\beta(I_0 - 1)^\beta)}.$$

Lines: 233-234: The first-order sensitivity index is given by:

$$S_i = \frac{V_i}{V}.$$

(2) 107: The constitutive model is not fully clear to someone not familiar with the specific model. What is the strain-like variable (λ_n , what exactly is λ_n ?) and how is that generalized to 3D problems as simulated in the examples? What are I_n , I_0 . The model seems also overly complex, if this is standard, a reference would be nice.

- We greatly thank the Reviewer for this valuable comment. We have revised the manuscript to explicitly define the strain-like variable λ_n . We also clarified the model's origin and provided references to standard implementations. Specifically, the scalar λ_n represents the fiber stretch ratio, defined as the ratio of the current fiber length to its reference (unstressed) length along the fiber direction. The related invariant I_n corresponds to the square of the fiber stretch ratio, $I_n = \lambda_n^2$. A threshold value $I_0 = \lambda_0^2$ defines the transition from the nonlinear toe region to the linear region of the material response. This model is widely used in soft tissue biomechanics, and implemented in the FEBio software as the *fiber-exp-pow-linear* material. For more detailed background, we include appropriate references. The revisions we performed are as follows:

Lines 121-134: The scalar quantity λ_n represents the fiber stretch ratio, defined as the ratio of the current fiber length to its reference length. The related invariant I_n corresponds to the square of the fiber stretch ratio, $I_n = \lambda_n^2$. A threshold value $I_0 = \lambda_0^2$ defines the transition from the nonlinear toe region to the linear region of the material response. The coefficients ξ and B are defined to ensure continuity of the strain energy function:

$$\xi = \frac{E_f(I_0 - 1)^{2-\beta} \exp[-\alpha(I_0 - 1)^\beta]}{4I_0^{3/2}(\beta - 1 + \alpha\beta(I_0 - 1)^\beta)},$$

$$B = E_f \frac{2I_0 \left(\beta - \frac{1}{2} + \alpha\beta(I_0 - 1)^\beta \right) - 1}{4I_0^{3/2}(\beta - 1 + \alpha\beta(I_0 - 1)^\beta)}.$$

In-vitro measurements showed that λ_0 is approximately 1.01 and assumed to be a fixed parameter. For this material type, the fiber modulus at the strain origin reduces to zero unless $\beta = 2$. Thus, we set $\beta = 2$ in the *in-silico* simulation. In summary, the matrix is assumed to exhibit viscoelastic

behavior, while the fiber is modeled as a viscoelastic component that provides tensile reinforcement, using the **fiber-exp-pow-linear** material model available in FEBio. This approach captures both the time-dependent behavior and the load-bearing property of the fibers within the composite tissue. For additional theoretical background, see [36, 37].

(3) 116: "the fiber is modeled as a fiber reinforced viscoelastic material" - that is not straightforward to understand

- We thank the Reviewer for the constructive comment regarding the description of the fiber behavior. We agree that the previous wording may have been unclear. To clarify, we have revised the manuscript to explicitly state that the matrix is assumed to exhibit viscoelastic behavior, while the fiber is modeled as a viscoelastic component that provides tensile reinforcement, using the **fiber-exp-pow-linear** material model available in FEBio. This approach captures both the time-dependent behavior and the load-bearing property of the fibers within the composite tissue.

The manuscript has been updated accordingly as follows:

Lines 130-134: In summary, the matrix is assumed to exhibit viscoelastic behavior, while the fiber is modeled as a viscoelastic component that provides tensile reinforcement, using the **fiber-exp-pow-linear** material model available in FEBio. This approach captures both the time-dependent behavior and the load-bearing property of the fibers within the composite tissue.

(4) Table 1: Estimating the relaxation times and the amplitudes at the same time is generally a difficult ill-posed problem and in many cases people use a fixed set of retardation times covering the time interval of interest (e.g. <https://doi.org/10.1016/j.compstruc.2014.01.024>). It would be interesting to discuss what is happening when just fixing those to specific values (e.g. with a factor of 10, so 1, 10, 100), which is somehow what the priors indicate as well. For higher precision, this interval could be reduced, e.g. 1,2,4,8,16,.. This would decrease the number of parameters to be estimated.

- We thank the Reviewer for this valuable comment. We agree that simultaneously estimating relaxation times and amplitudes can lead to an ill-posed problem. We discussed the alternative strategy as suggested by the Reviewer. To assess the effect of fixing relaxation times, we performed two optimization runs for the same specimen. In the first case, we considered all 16 parameters (including three relaxation times and three amplitudes for both fiber and matrix). In the second case, we fixed the relaxation times to $\tau_1 = 1$ s, $\tau_2 = 10$ s, and $\tau_3 = 100$ s for both constituents, reducing

the number of free parameters to 9. We included the updated parameter sets and the minimum values of $f(x)$ obtained via BO for each case in a supportive file (*supportive_file_graphs_set.pdf*). The file contains **Case I Graphs (Pages 1–101)** and **Case II Graphs (Pages 102–202)**. The optimal parameter sets for each case are also duplicated at the end of the document for convenience. The results showed that the minimum objective values were $f(x) = 22.8866$ N (Page 96 and 101, call no at 95) for the full parameter set and $f(x) = 24.8891$ N (Page 127 and 202, call no at 25) for the fixed relaxation time case, indicating that the performance difference was minor. These results support the Reviewer’s suggestion that fixing the relaxation times can be an appropriate strategy. We have added a corresponding discussion and cited the relevant literature in the revised manuscript.

Lines 476–480: We note that, while the model includes both viscoelastic amplitudes and their corresponding relaxation times as free parameters, estimating both sets simultaneously can lead to an ill-posed problem. A common alternative is to fix the relaxation times to a predefined set of values (e.g., 1, 10, 100 s) that span the relevant time scales [49]. This approach reduces parameter dimensionality and computational cost.

(5) Fig 2: The symmetry bc are not illustrated along the complete line of symmetry. It is also not clear if this is axisymmetric or a 2D model with plane stress/plane strain assumptions. The test photo also seems to have rigid loading platens, which means the top loading is displacement controlled (all have the same displacement). In that case, the model seems to have more axis of symmetry.

- We thank the Reviewer for this valuable comment. To reduce computational cost, the sample is modeled using a single 3D hexahedral element, with symmetry imposed in the y -direction by constraining the left face ($u_y(t) = 0$), as illustrated in Figure 2. The bottom nodes are constrained in the vertical direction ($u_z(t) = 0$), and the top nodes are subjected to displacement-controlled loading using the measured displacement $u_z(t)$, consistent with the *in-vitro* test protocols. The Reviewer is correct that, in principle, an additional axis of symmetry could be applied along the x -direction. However, in this study, we applied symmetry only along the y -axis to simplify the model setup. We confirm that the model is not axisymmetric or a 2D model with plane stress/plane strain assumptions; it is a 3D model implemented using a single hexahedral element. In the revised manuscript and Figures 2 and 3, we clarified the imposed symmetry boundary conditions for this

3D configuration. The revised text appears in the manuscript as follows:

Lines 142:146: To reduce computational cost, the sample is modeled using a single 3D hexahedral element, with symmetry imposed in the y -direction by constraining the left face ($u_y(t) = 0$), as shown in Figure 2. The bottom nodes are constrained vertically ($u_z(t) = 0$), and the top nodes are displacement-controlled using measured displacements $u_z(t)$, consistent with the *in-vitro* test protocols.

(6) 151: How did you chose the hyperparameters of the kernel in the BO, in particular the correlation length? What kernel did you use, and how did you consider the different dimensions (scaling? Isotropic kernel?) How did you start the process (was there some initial random sampling or DOE schema used?)

- We greatly thank the reviewer for this constructive comment. We have now included the relevant implementation details in the revised manuscript to clarify the kernel choice, length-scale handling, and initialization approach. In our implementation using the `scikit-optimize` library, we employed a Gaussian Process (GP) surrogate model with a Matérn kernel. The kernel was used in its anisotropic form, meaning that a separate length-scale was automatically estimated for each input dimension. This allows the GP to adapt to varying sensitivities across parameters. The length-scale hyperparameters were not manually set; instead, they were learned during the fitting process through internal maximization of the marginal likelihood using the default optimizer provided by `scikit-optimize`. We did not apply a specific design of experiments (DOE) scheme for initialization. Instead, the optimization process was initialized using random sampling strategy to generate the initial points before the updates. This approach provides unbiased coverage of the search space and is commonly used for black-box optimization problems where prior knowledge of the objective landscape is limited. We have included the following statement in the revised manuscript:

Lines 169-172: In this study, the surrogate model was built using a Gaussian Process (GP) with a Matérn kernel, as provided by the `scikit-optimize` library. An anisotropic kernel was used, allowing a separate length-scale to be estimated for each parameter dimension. The optimization process was initialized using random sampling strategy.

(7) 163: The stopping criteria seems very problem specific. Why didn't you choose something like a threshold on the expected improvement?

- We thank the Reviewer for this thoughtful suggestion. We agree that using a threshold can

provide a more adaptive and theoretically grounded stopping criterion. However, in our setting, we found that using a fixed number of iterations ensured predictable computational cost and yielded consistent results across specimens. In preliminary tests, employing a threshold led to extended runtimes without notable improvements in accuracy. Therefore, we opted for a fixed-iteration approach for practical and computational efficiency. We now clarify this rationale in the revised manuscript. Additionally, we include the updated parameter sets sampled during BO, the corresponding experimental vs. numerical curves, and the minimum value of $f(x)$ achieved within 100 iterations (please see Case I Graphs, Pages 1–101 given in Supporting File "supportive_file_graphs_set.pdf"). We believe this fixed-iteration strategy is reasonable for our implementation.

Lines 184-190: We empirically observed that a fixed stopping criterion of 100 iterations provided sufficient convergence for the calibration of specimen-specific parameters. While adaptive criteria, such as convergence thresholds, may be more theoretically grounded, we found that using a fixed number of iterations ensured predictable computational costs and produced consistent results across specimens in our setting. In preliminary tests, threshold-based stopping led to extended runtimes without significant gains in accuracy. Therefore, we adopted a fixed-iteration approach for practical and computational efficiency.

(8) 212: The Sobol indices depend on the parameter (prior) distributions. How are they chosen, since in this setup the uniform priors are obtained as the deterministic parameters for the different samples. That itself might be already an ill-posed inverse problem where the maximum that you used might not be a good indicator of the actual distribution, in particular if the posterior is multimodal.

· We greatly thank the reviewer for this insightful and important comment. In our Saltelli-based Sobol sensitivity analysis, we used uniform distributions over the parameter ranges defined in Table 1. These ranges were informed by the Bayesian Optimization (BO). We fully agree that using uniform priors, although a common practice in variance-based sensitivity analysis, may not adequately capture the true posterior distribution—especially in cases where the parameter space is multimodal. This simplification may lead to biased or less informative sensitivity indices. To address this important point, we have revised the manuscript to explicitly state our assumptions, explain the potential limitations of uniform sampling. We have also noted that future work could benefit from incorporating posterior-based sampling strategies to enhance the fidelity of sensitivity

estimates. The following changes were made in the manuscript:

Lines 242-249: In our Saltelli-based Sobol sensitivity analysis, we employed uniform distributions over the parameter ranges as defined in Table 1. These ranges were initially informed by the results of the Bayesian Optimization (BO). While using uniform priors over these ranges enables non-informative sampling and is a common practice in variance-based sensitivity analysis, we acknowledge the limitations of this approach. Specifically, this choice may not capture the true posterior distributions of the parameters — particularly if the underlying parameter space is multimodal or exhibits strong correlations. Future work could involve using posterior-informed distributions to improve the fidelity of sensitivity estimates.

(9) 224: ABC with a Gaussian kernel and Euclidean distance and a deterministic forward model is equivalent to standard Bayesian inference with additive Gaussian noise of variance ϵ^2 . In your case, this could also be a latent variable that you infer.

- We thank the reviewer. We agree that, in the case of a deterministic forward model using a Gaussian kernel with Euclidean distance, ABC is mathematically similar to standard Bayesian inference with additive Gaussian noise of variance ϵ^2 . In our implementation using PyABC, we treat ϵ as an adaptively decreasing threshold that determines which simulated data points are considered sufficiently close to the observed data, as part of the Sequential Monte Carlo (SMC) procedure. We have revised the manuscript to acknowledge this equivalence and to note that future work could involve inferring ϵ as a latent variable to better capture observations. The following sentences has been added to the manuscript:

Lines 298-301: While our current implementation treats ϵ as a fixed threshold that is adaptively decreased within the Sequential Monte Carlo (SMC) procedure of PyABC, future work could involve treating this tolerance as a latent variable and inferring it jointly with the model parameters to better reflect observations.

(10) 236: Why do you use a uniform kernel rather than a Gaussian kernel? So $K(\epsilon) = \exp(-d(y, y_{\text{obs}})^2/\epsilon^2)$, and in particular, how do you estimate ϵ , since that is somehow related to your noise level. For deterministic models, the posterior distribution in ABC methods converges to point estimates for $\epsilon > 0$, for larger epsilon a larger variance is obtained. However, since epsilon is randomly chosen (as small as possible, but still computationally feasible to avoid rejecting all samples?) the obtain variance in the posterior depending on epsilon is also just random (based on the choice of

epsilon). What is then the physical interpretation of the uncertainties that are obtained with ABC sampling in the posterior e.g. related to the predictive distributions that you plot in e.g. Fig 3. That is also true for the conclusion you draw in line 368, which I would not support.

- We greatly thank the reviewer for this insightful and technically relevant comment. In our implementation using the PyABC library, we employed hard-threshold (indicator) kernel defined as $K_\varepsilon = I(d(y_{obs}, y_{sim}) \leq \varepsilon)$ where $d(,)$ denotes the Euclidean (L2) distance. This does not correspond to a uniform kernel over the distance, but rather a uniform acceptance region within a tolerance ε . We acknowledge the potential confusion and would like to clarify that the prior distributions for the model parameters (as shown in Table 1) were specified as uniform, which is distinct from the kernel used for accepting or rejecting samples in the ABC procedure. Regarding ε , it was initialized at a reasonable value based on pilot trials and automatically adapted via the built-in Sequential Monte Carlo (SMC) schedule in PyABC. We agree with the reviewer that in the limit $\varepsilon \rightarrow 0$, the ABC posterior collapses to a point estimate in deterministic models, whereas larger values could yield a broader posterior. As for the physical interpretation of the predictive uncertainty bands shown in Fig. 3 and Fig. 12, we emphasize that: these bands reflect parameter uncertainty—that is, the variation in posterior samples accepted under the ABC threshold. All predictive variability arises from uncertainty in parameter estimates, not from model noise. This uncertainty reflects the inter-individual biological variability across specimens. In Fig. 3, the upper figures show the applied loading conditions, the middle figures present the specimens' experimental stress responses, and the bottom figures display the predicted stress bands derived from ABC posterior samples. We note that Figure 3 is included primarily to illustrate the implementation procedure, demonstrating how ABC interacts with the simulator and experimental observations. A more detailed presentation of the inferred simulations from the ABC posterior samples, along with the experimental observations, is given in Figure 12. As seen, even under similar specimen geometries, the experimental stress responses exhibit significant variability—likely driven by age, tissue health, donor-specific factors, or anatomical heterogeneity. Therefore, we interpret the posterior uncertainty as a plausible range of model outcomes consistent with observed variability in the data.

(11) 277: In your approach, you use the data multiple times, once to compute the prior using BO), and then once again in your ABC method. From a pure Bayesian perspective this is wrong, since it

biases the results (prior means prior because this is the knowledge without the data). In particular, the number of data points in standard Bayesian setting determines the posterior variance, thus if you double the number of data points, you get smaller variances. As such, your actual posterior is probably wider. Fig. 3 it would be nice to plot exp. and simulation in the same plot to allow a comparison. What are the bounds in the numerical model (mean and min/max or \pm std_dev, or 95% interval)?

· We thank the reviewer for this important and valid observation regarding the construction of priors based on data-informed procedures. Our intention in this study was to derive practical bounds for the parameters, informed by domain knowledge and preliminary fits (via BO), to ensure efficient sampling in ABC within plausible physiological ranges. While this data-informed prior improves computational feasibility, we fully agree that it does not represent a fully independent prior in the classical Bayesian sense. To clarify this limitation and remain transparent, we have revised the manuscript to explicitly state that the priors were informed by exploratory analyses and acknowledge that this may lead to an underestimation of the true posterior variance. We have also added a discussion noting that future work should consider truly prior-knowledge-based bounds or hierarchical ABC Bayesian models, where uncertainty in the prior can be treated more rigorously. We again note that Figure 3 is included primarily to illustrate the implementation procedure, demonstrating how ABC interacts with the simulator and experimental observations. A more detailed presentation of the inferred simulations from the ABC posterior samples, along with the experimental observations, is provided in Figure 12. We also report the mean, standard deviation, and 95% HDI of the posterior parameters in Table 3. These points have been clarified in the revised manuscript as follows:

Lines 290-294: In this study, the prior distributions for the parameters are defined based on a uniform distribution (Table 1). We note that these priors were informed by initial exploratory analyses and preliminary specimen-specific calibrations using Bayesian optimization (BO). While this approach improves sampling efficiency by focusing on physiologically plausible ranges, it does not constitute a strictly prior-knowledge-based prior in the classical Bayesian sense.

Lines 510-525: This study shows that the parameters calibrated using the probabilistic technique (Table 3) differ from those obtained through the frequentist approach (Table 2). In the frequentist approach, we optimize parameters separately for each specimen based on its own data

using Bayesian Optimization (BO). In contrast, in the ABC approach, we use data from all specimens collectively to infer posterior parameter distributions, capturing uncertainty in the estimates. For example, consider the elastic modulus of fiber E_f for the distal site: using the frequentist approach, the average E_f value for nine specimens is 204.82 ± 27.42 MPa (mean \pm standard deviation), whereas the ABC estimate is 216.2 ± 31.12 MPa. While this difference illustrates how inference outcomes may vary between methods, it should be interpreted with caution due to key modeling assumptions. For instance, the prior ranges used in the ABC framework were informed by the parameter bounds of BO calibration. Although the observations used in BO and ABC differ, this approach introduces a form of indirect data reuse that may lead to underestimation of posterior uncertainty. Future work should consider using hierarchical ABC models or priors based on external domain knowledge to reduce this potential bias. Similarly, the initial choice of $\epsilon = 0.3$ was made empirically. While the ABC-SMC algorithm adaptively updates this threshold in later generations, the initial value still reflects a modeling decision that may influence the resulting posterior distributions.

(12) 344: the first order sobol indices usually sum up to something smaller than 1, that seems not the case in the results in Fig 10. why?

· We sincerely thank the reviewer for this critical and constructive comment. Upon reviewing our analysis, we identified that the observed inconsistency—where the sum of the first-order Sobol indices exceeded 1—was caused by irregularities in the model output. Specifically, the output displayed non-smooth behavior, which can violate the assumptions of Sobol sensitivity analysis. To resolve this, we employed a nearest neighbor interpolation approach to approximate the model output over (objective function) the input space (parameters). This surrogate method effectively smoothed the response output, thereby allowing for a more stable and consistent variance decomposition. As a result, the recalculated first-order Sobol indices now sum to a value below 1, consistent with theoretical expectations. We would like to express our deep gratitude to the reviewer for highlighting this issue. Without this observation, we would not have detected this subtle but important flaw. Your feedback directly contributed to improving the robustness of our sensitivity analysis. As supporting context, surrogate modeling approaches are commonly used in global sensitivity analysis to handle or non-smooth model outputs. The following statements have included in the revised manuscript. Additionally, the figure 10 that represent the Sobol sensitivity is updated.

Lines 250-264: To ensure stable and theoretically consistent sensitivity index computation, we implemented a normalization strategy for all 16 input parameters. Each parameter was scaled to the [0,1] interval based on its empirical minimum and maximum values across the dataset. This step not only facilitates variance-based decomposition but also helps avoid scale-related instabilities. The model output used for Sobol analysis was the total error function defined in Eq. 9 which aggregates discrepancies across three experimental loading scenarios. During our initial analysis, we observed that the sum of first-order Sobol indices occasionally exceeded 1, which violates theoretical expectations for additive variance decomposition. We identified that this issue was caused by non-smooth behavior in the output space. To address this, we employed a surrogate modeling strategy using a nearest-neighbor interpolation method. Specifically, Saltelli-generated samples were projected into the empirical parameter space by finding the closest real data points in a normalized feature space. The associated output values from these matched samples were then used for computing Sobol indices. The use of surrogate modeling is a standard remedy for non-smooth or computationally expensive models in global sensitivity analysis and has been recommended in several studies [44, 45]. Additional details on the Sobol sensitivity analysis are reported in the previous study [46].

Lines 396-400: Similar to the results obtained from the random forest analysis, E_f , E_m , and α_f are identified as the most sensitive parameters in the model. The total and first-order sensitivity indices for these parameters are presented in Figure 10. Based on the total-order index scores, the three most sensitive parameters, in descending order, are: E_f (0.7325), E_m (0.4905), and α_f (0.3587).

Lines 486-487: Third, sensitivity analysis and feature importance showed that E_f , α_f , and E_m parameters have the highest influence on the model.

(13) 355: does 40 mean 40 accepted, or 40 in total? epsilon 0.3 is relatively large, how was that chosen (see similar question before)?

· We thank the reviewer for this comment. To clarify, the number 40 refers to the population size per generation in the ABC Sequential Monte Carlo (SMC) algorithm. Each generation includes 40 accepted sample sets that satisfy the distance criterion $d(y_{obs}, y_{sim}) \leq \varepsilon$ with the initial

tolerance set to $\varepsilon = 0.3$. We have revised the manuscript to clarify this point.

Lines 408-410: The ABC inference is initiated with a tolerance threshold of $\epsilon = 0.3$, selected empirically to allow for sufficient sampling diversity in the initial generation. This threshold is adaptively updated by the ABC-SMC algorithm in subsequent populations, progressively tightening the acceptance criterion around the observed data. In each generation, 40 accepted sample sets are retained.

(14) 455: See the comments related to using the data twice and the choice of epsilon, I think the probabilistic conclusion that are drawn here strongly depend on these (arbitrary) assumptions and I would be very cautious in the generalization.

· We thank the reviewer again for this important point. We fully acknowledge that the probabilistic conclusions drawn from the ABC approach—specifically the comparison between posterior estimates and frequentist results—are influenced by both the data-informed construction of the prior and the choice of the initial tolerance threshold ε . In response, we have revised the manuscript to clarify that the observed differences should be interpreted in light of these modeling assumptions. The updated statements are as follows:

Lines 510-525: This study shows that the parameters calibrated using the probabilistic technique (Table 3) differ from those obtained through the frequentist approach (Table 2). In the frequentist approach, we optimize parameters separately for each specimen based on its own data using Bayesian Optimization (BO). In contrast, in the ABC approach, we use data from all specimens collectively to infer posterior parameter distributions, capturing uncertainty in the estimates. For example, consider the elastic modulus of fiber E_f for the distal site: using the frequentist approach, the average E_f value for nine specimens is 204.82 ± 27.42 MPa (mean \pm standard deviation), whereas the ABC estimate is 216.2 ± 31.12 MPa. While this difference illustrates how inference outcomes may vary between methods, it should be interpreted with caution due to key modeling assumptions. For instance, the prior ranges used in the ABC framework were informed by the parameter bounds of BO calibration. Although the observations used in BO and ABC differ, this approach introduces a form of indirect data reuse that may lead to underestimation of posterior uncertainty. Future work should consider using hierarchical ABC models or priors based on external domain knowledge to reduce this potential bias. Similarly, the initial choice of

$\epsilon = 0.3$ was made empirically. While the ABC-SMC algorithm adaptively updates this threshold in later generations, the initial value still reflects a modeling decision that may influence the resulting posterior distributions.

Reviewer #2

The manuscript focuses on developing a Bayesian framework for the identification of soft tissues. It is well-written, and my comments/questions are as follows:

- We sincerely thank the Reviewer for the constructive comments, suggestions, and feedback,

which significantly improved this manuscript. We revised our manuscript in accordance with the Reviewer's suggestions. The changes we made to the revised manuscript are presented in red color.

(1) The concept of Bayesian inference for solid mechanics and soft tissues is rather well-established.

I fail to see most of the significant references that should be mentioned in this work, such as:

TheThe Madireddy et al., "A Bayesian approach to selecting hyperelastic constitutive models of soft tissue" (2015)

Madireddy et al., "Bayesian calibration of hyperelastic constitutive models of soft tissue" (2016)

J.T. Oden et al., "Selection and assessment of phenomenological models of tumor growth" (2013)

Chiachío J. et al., "Bayesian model selection and parameter estimation for fatigue damage progression models in composites" (2015)

Rappel et al., "A Tutorial on Bayesian Inference to Identify Material Parameters in Solid Mechanics" (2020)

Rappel et al., "Identifying elastoplastic parameters with Bayes' theorem considering output error, input error, and model uncertainty" (2019).

Haughton, "Bayesian Inference on Microstructural, Hyperelastic Models of Soft Tissue Deformation" (2022)

And most of the work done by James Beck on the identification of solid mechanics. Therefore, I suggest a more comprehensive literature review on BI for the introduction.

Continuing on my previous comment, I fail to understand how this work differentiates itself from previous works. Perhaps the author can clarify this in a paragraph.

- We thank the reviewer for pointing out this important oversight. We agree that Bayesian inference (BI) in solid mechanics and soft tissue modeling is well-established, and we have now significantly expanded the introduction to acknowledge and cite key foundational contributions. Specifically, we have added references to the suggested works by Madireddy et al. (2015, 2016), Oden et al. (2013), Chiachío et al. (2015), Rappel et al. (2019), Haughton et al. (2022), and others by James Beck and colleagues in structural mechanics. These studies have significantly contributed to the development of Bayesian calibration, model selection, and uncertainty quantification techniques in biomechanics and related fields. We have also added a clarifying paragraph to the *Introduction* to better differentiate our work from these prior efforts. While previous studies typically apply standard Bayesian methods with an explicit likelihood function or rely on surrogate models for likelihood evaluation, our study contributes by demonstrating the application of likelihood-free Bayesian inference (ABC) directly coupled with high-fidelity in-silico simulation for soft tissues, where the likelihood is intractable. The following statements are included in the revised manuscript.

Lines 40-70: Furthermore, several studies have established the utility of Bayesian inference in solid mechanics and soft tissues, addressing both parameter estimation and model selection. For instance, Madireddy et al. [15, 19] presented a Bayesian model selection and calibration framework for hyperelastic soft tissue models. Haughton et al. [20] used Bayesian techniques to quantify uncertainty in microstructural tendon models. Oden et al. [21] and Chiachio et al. [22] implemented Bayesian methods for selecting and validating phenomenological and damage progression models. Rappel et al. [23] provided detailed frameworks to identify the parameters of the elastoplastic material under uncertainty. In addition, James Beck and colleagues have applied Bayesian learning to structural health monitoring and inverse problems in mechanics [24, 25, 26, 27]. Furthermore, Babuska et al. [28] presented a Bayesian model comparison approach for metallic fatigue data, while Xue et al. [29] proposed sparse Bayesian learning framework for robust damage localization using guided-wave testing. These studies primarily rely on standard Bayesian frameworks that require an explicit likelihood function or surrogate-assisted inference. However, the likelihood function can be difficult or computationally expensive to derive for nonhomogeneous materials under complex biomechanical loading conditions. To overcome these such issues, an approximate Bayesian computation (ABC) approach that does not use the likelihood function has been proposed [30, 31] and implemented recently in some fields including structural health monitoring [32] medical decision

making [33] and operation research management [34]. However, the coupling of in-silico simulations for stochastic calibration and uncertainty quantification using likelihood-free Bayesian computation in the field of mechanics of biological materials with high inter-specimen variability has been largely unaddressed to date, to the best of our knowledge. The most attractive aspect of this approach is that the likelihood function is not required to be explicitly represented in a closed analytical form. Once an in-silico model is built to mimic the *in-vitro* conditions, it directly bypasses the need for explicit likelihood evaluation and relies on comparing the simulated data from the *in-silico* model with experimental observations from the *in-vitro* test. This approach can be implemented in a wide range of *in-vivo* and *in-vitro* applications, ranging from predicting the mechanical characteristics change of tissue due to the risk of pathogenic disease to planning surgical procedures. We note that this study is not targeted to develop or present a constitutive material model for connective tissue, but rather to show how likelihood-free inference can be used directly with the numerical simulator and measurements. Any suggested model can be directly embedded in the simulator.

(2) Section 2.3: Are the mechanical properties considered to be uniform across the test specimen? If yes, why not make it a random field? If they are considered as random fields, how are they modeled? Please clarify.

- We greatly thank the Reviewer for this point. In our study, the mechanical properties are assumed to be homogeneous and spatially uniform throughout the specimen. That is, each material parameter (e.g., modulus, viscoelastic constants) is represented by a single scalar value per specimen. This modeling choice is primarily motivated by the available experimental data and the goal of calibrating a specimen-specific but spatially averaged material behavior. Accordingly, we performed Bayesian optimization to determine specimen-specific parameter values, and inform ABC for uncertainty quantification. The parameter search ranges used during BO are given in Table 1. These ranges were initialized as follows: the viscoelastic characteristics g_i and τ_i were first estimated by fitting trial one-step relaxation measurements using the Levenberg–Marquardt method. The resulting parameter bounds were extended and used as search intervals in BO. Similar procedures were followed for the fiber and matrix components. For an approximate modulus estimate, we evaluated the linear region of a typical incremental cyclic loading measurement, which suggested an overall composite modulus of approximately 350 MPa. Although to our knowledge no study has directly measured the fiber and matrix moduli of human Achilles tendon separately, some

rat studies have reported fiber-to-matrix ratios between 5 and 10. In this study, the prior distributions for ABC are uniform over the ranges in Table 1. These priors were informed by exploratory analyses and preliminary specimen-specific calibrations using BO. While this improves sampling efficiency, it does not constitute a strict prior-knowledge-based prior in the classical Bayesian sense. The following statements are included in the manuscript.

Lines 201-211: The parameter search ranges used during BO are given in Table 1, and the initial search ranges for these parameters are predicted as follows. First, the viscoelastic characteristics g_i and τ_i are estimated by fitting on some trial one-step relaxation measurements using the Levenberg-Marquardt method. Then, the bounds of the estimated parameters are extended and used as search ranges for BO. Similar search ranges are considered for the fiber and matrix components. For the approximate prediction of the modulus, we initially evaluated it by analyzing the linear region of a typical incremental cyclic test loading measurement and found that the modulus of elasticity for the composite tendon (matrix + fiber) is around 350 MP. Although, to the best of our knowledge, no study has experimentally quantified the elastic modulus of the fiber and elastic component in the human Achilles tendon separately, it has been stated in some rat studies that the fiber-to-matrix ratio is between 5 and 10 [39, 40, 41].

Lines 290-294: In this study, the prior distributions for the parameters are defined based on a uniform distribution (Table 1). We note that these priors were informed by initial exploratory analyses and preliminary specimen-specific calibrations using Bayesian optimization (BO). While this approach improves sampling efficiency by focusing on physiologically plausible ranges, it does not constitute a strictly prior-knowledge-based prior in the classical Bayesian sense.

(3) Section 2.4: It needs to be justified why the author is using BO (Bayesian Optimization). I understand that this is to reduce the computational cost; however, this is not clarified in the text.

- We thank the Reviewer for this important observation. We have now explicitly clarified in the revised manuscript that Bayesian Optimization (BO) was used due to the high computational expense of finite element simulations, which makes standard optimization approaches impractical. Additionally, we note that BO served two main purposes in our study: (i) to identify specimen-specific parameters efficiently for use in finite element model calibration, and (ii) to define informative parameters for the ABC framework. Furthermore, BO allowed us to compare frequentist point estimates with posterior distributions derived from ABC, facilitating a direct comparison between

deterministic and probabilistic inference methods. These clarifications have now been included to the manuscript as follows.

Lines 153-160: BO was selected primarily due to the high computational cost of finite element simulations involved in evaluating the objective function $f(x)$. Each evaluation requires solving a full-scale FE model, making traditional methods such as grid search or evolutionary algorithms computationally impractical. Beyond efficient parameter calibration, BO also served two purposes in this study: (i) to inform the parameter ranges used as priors in the ABC-based uncertainty quantification framework, and (ii) to compare frequentist estimates obtained from BO with probabilistic posteriors derived from ABC, thus enabling a direct comparison between deterministic and stochastic inference approaches.

Lines 349-352: Figure 4 shows that the minimum $f(x)$ function converges rapidly, even with only a few initial iterations. This characteristic makes BO popular in machine learning for hyper-parameter optimization, where the learning algorithm is treated as a black-box function.

Lines 510-525: This study shows that the parameters calibrated using the probabilistic technique (Table 3) differ from those obtained through the frequentist approach (Table 2). In the frequentist approach, we optimize parameters separately for each specimen based on its own data using Bayesian Optimization (BO). In contrast, in the ABC approach, we use data from all specimens collectively to infer posterior parameter distributions, capturing uncertainty in the estimates. For example, consider the elastic modulus of fiber E_f for the distal site: using the frequentist approach, the average E_f value for nine specimens is 204.82 ± 27.42 MPa (mean \pm standard deviation), whereas the ABC estimate is 216.2 ± 31.12 MPa. While this difference illustrates how inference outcomes may vary between methods, it should be interpreted with caution due to key modeling assumptions. For instance, the prior ranges used in the ABC framework were informed by the parameter bounds of BO calibration. Although the observations used in BO and ABC differ, this approach introduces a form of indirect data reuse that may lead to underestimation of posterior uncertainty. Future work should consider using hierarchical ABC models or priors based on external domain knowledge to reduce this potential bias. Similarly, the initial choice of $\epsilon = 0.3$ was made empirically. While the ABC-SMC algorithm adaptively updates this threshold in later generations, the initial value still reflects a modeling decision that may influence the resulting posterior distributions.

(4) Section 2.5: One or two sentences are needed about standard Bayesian inference (BI). Unless readers are already in the field, they won't know why the author has decided to use ABC (approximate Bayesian computation) and how it differs from standard Bayesian inference.

- We thank the Reviewer for this helpful comment. We have now added a brief clarification in the ABC section to explain how ABC differs from BI. The revised statements in the manuscript are as follows:

Lines 266-280: Although the standard Bayesian framework allows for updating prior beliefs about parameters based on the likelihood of the data given those parameters, evaluating the likelihood $P(\mathbf{y}_{\text{obs}}|\boldsymbol{\theta})$ is often infeasible, but the model can generate synthetic data \mathbf{y}_{sim} given parameters $\boldsymbol{\theta}$. In general, Bayesian inference provides a principled framework for quantifying uncertainty in model parameters by combining prior knowledge with evidence from observed data through the likelihood function. However, for many nonlinear models, deriving an analytical or tractable likelihood function is difficult or impossible. Here, we implemented likelihood-free approximate Bayesian computation (ABC) for stochastic calibration and uncertainty quantification of posterior parameters using PyABC [31]. The framework is based on an executable "black-box" forward process model that simulates data using given model parameters [47, 48]. In ABC, the computation of the likelihood is replaced by the comparison between observed (*in-vitro* measurements) \mathbf{y}_{obs} and simulated data (*in-silico* simulations) \mathbf{y}_{sim} . Given the prior distribution of $P(\boldsymbol{\theta})$ of parameters $\boldsymbol{\theta}$, the target is to approximate the posterior distribution $P(\boldsymbol{\theta}|\mathbf{y}_{\text{obs}})$ given observed data \mathbf{y}_{obs} , a model $f(\mathbf{y}_{\text{sim}}|\boldsymbol{\theta})$, and a prior distribution $P(\boldsymbol{\theta})$. Typically, it is based on generating simulated data \mathbf{y}_{sim} for parameters $\boldsymbol{\theta}$ drawn from the prior distribution and retaining parameters for which \mathbf{y}_{sim} is sufficiently close to \mathbf{y}_{obs} .

(5) Further explanation on ABC is necessary. What is the algorithm? How are the computations done, etc.?

- We thank the reviewer for this insightful comment. In the revised manuscript, we have substantially expanded the section on Approximate Bayesian Computation (ABC) to clarify the algorithm and computational procedures used in our study. We now provide a more comprehensive explanation of the motivation for using ABC. The revised text introduces the mathematical formulation of ABC, where the posterior distribution is approximated by accepting parameter samples for which the simulated data closely matches the observed data within a specified tolerance threshold. We

illustrate the implementation procedures of ABC in Figure 3. We define the key components of this framework, including the distance metric, tolerance level, and indicator function (Eq. 15) and explain that the Euclidean (L2) norm is used to quantify the discrepancy between simulated and observed data. To improve computational efficiency and accuracy, especially given the high-dimensional parameter space and potentially low acceptance rates for small tolerance values, we adopted a Sequential Monte Carlo (SMC) approach implemented through the PyABC library. This method adaptively refines the posterior approximation by progressively lowering the tolerance threshold ε across generations, enabling more efficient exploration of the parameter space. We also clarified that the prior distributions for the parameters are defined as uniform, with bounds informed by exploratory Bayesian optimization results, which focus the sampling on physiologically plausible regions. We believe these additions, which are now included in the revised manuscript (Lines: 266-301), directly address the reviewer's request for a clearer explanation of the algorithm and the computational steps involved. The updated statements for the implementation procedures are as follows:

Lines 319-345: The implementation procedure and sequence of steps illustrated in Figure 3 are as follows:

1. *In-vitro* test samples are harvested and re-sectioned into an appropriate shape for the biomechanical test. A higher number of samples allows for better quantification.
2. *In-vitro* biomechanical tests are performed to obtain output observations. Here, the resulting reaction forces $R(t)$ are referred to as \mathbf{y}_{obs} . As an addendum to the one-step and two-step relaxation loadings, we include only single-cycle observations (loading-unloading) from the incremental cyclic test during ABC inference.
3. The importance and sensitivity of each parameter are determined using the Random Forest and Sobol methods. Once the minimum and maximum bounds obtained from BO across all samples are determined, these wide bounds are used as priors in ABC. Initially, parameters $\boldsymbol{\theta}$ are drawn from the prior uniform distribution as: $\boldsymbol{\theta} \sim P(\boldsymbol{\theta})$.
4. The next step is to perform forward simulations to drive ABC. We implemented FEBio as the simulator and created a template that includes the FRVE material model and boundary

conditions that mimic the experiment. FEBio input files (.feb) are xml type files, and we used the `jinja` package to create the FEBio input template file and serialize the data between ABC and the simulator. Once ABC determines the input parameter set θ , it is passed directly to this simulator template, and the FEBio simulator generates simulated data $f(\mathbf{y}|\theta)$ using θ as: $\mathbf{y}_{\text{sim}} \sim f(\mathbf{y}|\theta)$.

5. The distance between the observed and simulated data is computed as: $d = d(\mathbf{y}_{\text{obs}}, \mathbf{y}_{\text{sim}})$, where $d(\cdot)$ is a Euclidean distance metric.
6. The parameter θ is retained if the distance satisfies: $d \leq \epsilon$; otherwise, return to step 4.
7. The joint plots of the posterior parameters are visualized, and the lower, mean and upper bounds, as well as the confidence interval 95% of the inferred simulation \mathbf{y}_{sim} , are plotted.

(6) How are the simulated data for equation 15 going to be produced?

- We thank the Reviewer for this important question. The simulated data \mathbf{y}_{sim} used in Equation 15 are generated through forward simulations performed using the finite element solver FEBio, which incorporates the fiber-reinforced viscoelastic (FRVE) material model and replicates the experimental boundary conditions. As described in the revised manuscript (Section: *Approximate Bayesian Computation*, Lines 266-301), once a candidate parameter set θ is sampled from the prior distribution, it is passed into a FEBio input template using a Python-based `jinja` package. The simulator then generates the corresponding synthetic reaction force responses \mathbf{y}_{sim} . These outputs are compared to the experimental measurements \mathbf{y}_{obs} using a Euclidean distance metric. If the distance satisfies the ABC acceptance criterion $d(\mathbf{y}_{\text{obs}}, \mathbf{y}_{\text{sim}}) \leq \epsilon$, the parameter θ is retained as a posterior sample. This process is iterated within the Sequential Monte Carlo (SMC) framework implemented via PyABC. The entire procedure is outlined step-by-step in Figure 3 and detailed in Lines 319-345 of the manuscript.

(7) How many specimens are used for specimen-specific parameter calibration? Has the author considered the population of these specimens?

- We thank the Reviewer for this insightful question. In total, 9 specimens were used for specimen-specific parameter calibration, with each specimen collected from three anatomical sites (distal, middle, and proximal), resulting in 27 unique site-specific datasets. Each of these datasets was

subjected to three loading protocols (one-step relaxation, two-step relaxation, and incremental cyclic), giving a total of 81 force-displacement curves for analysis. For Bayesian Optimization (BO), we performed specimen-specific parameter calibration. Specifically, for each anatomical site (distal, middle, proximal), all experimental observations from the one-step relaxation, two-step relaxation, and incremental loading-unloading tests were used to calibrate parameters for each specimen individually. In contrast, for Approximate Bayesian Computation (ABC), we did not perform specimen-specific analysis. Instead, we aggregated all measurements from multiple specimens at each site to perform population-level stochastic calibration. This approach enables the estimation of posterior parameter distributions while explicitly accounting for uncertainty across specimens. The statements regarding of this point are included in the manuscript as follows:

Lines 98-99: *In-vitro* measurements include 81 datasets (9 specimens x 3 sites x 3 test protocols).

Lines 152-154: To determine specimen-specific biomechanical parameters, Bayesian optimization (BO) is implemented using `scikit-optimize` library. BO was selected primarily due to the high computational cost of finite element simulations involved in evaluating the objective function $f(x)$.

Lines 319-322: The implementation of *in-vitro* measurements, coupled with *in-silico* simulation and ABC, resembles the BO stages at the pre-processing steps. However, the main difference is that instead of evaluating specimen-specific observations, ABC includes all specimens' measurements, allowing for the stochastic calibration of parameters, including uncertainty.

Lines 511-514: In the frequentist approach, we optimize parameters separately for each specimen based on its own data using Bayesian Optimization (BO). In contrast, in the ABC approach, we use data from all specimens collectively to infer posterior parameter distributions, capturing uncertainty in the estimates.

(8) Page 13: "We presented specimen-specific parameter identification results in the previous section and observed that the variability between samples is high and may be influenced by many factors..." How is this variability modeled? The uncertainty models can be due to noise, model error, and specimen variability; which one is modeled in this contribution, and why?

- We thank the Reviewer for this valuable question. In this study, we focused specifically on quantifying uncertainty arising from variability in mechanical parameters across specimens with

approximately similar geometry. We did not include uncertainty due to measurement noise, model-form error, or geometric differences. We acknowledge, however, the uncertainties can also arise from incomplete knowledge of the physical model, such as assumptions in initial/boundary conditions or simplifications in constitutive modeling. Nevertheless, as is common in biomechanics, our study—consistent with most existing literature—focuses on variability in material properties as the dominant source of uncertainty. Future extensions of this work could extend this approach by incorporating these additional sources of uncertainty. We also add this limitation in the manuscript. The following statements are included.

Lines 24-33: In addition to inhomogeneous characteristics, biological materials often exhibit intrinsic variability in their biomechanical response when subjected to external loads. The inter-subject or inter-specimen variability and uncertainty in biomechanical properties of these materials are high, which may be influenced by many factors such as the donor's age, genetics, the tissue's pathological state, gender, and other specific factors related to the tissue characteristics. For *in-vitro* samples, embalming medium, temperature, humidity, and duration are the additional factors that can affect the biomechanical properties. Oftentimes, *in-silico* model is hindered not only by the incompleteness of the theoretical approach but also by uncertainties due to mentioned factors that arise in the experimental observations. Thus, there is an urgent need to ensure that it can capture the intrinsic population of variability and not only be representative of 'mean' individuals.

Lines 402-406: We presented specimen-specific parameter identification results in the previous section and observed that the variability in mechanical parameters across samples is high, potentially influenced by factors such as donor age, genetics, tissue pathology, gender, and other sample-specific characteristics. To determine the uncertainty in these parameters and stochastically calibrate them, we implement likelihood-free inference in a probabilistic framework.

Lines 532-536: Finally, this study focused solely on quantifying uncertainty arising from variability in mechanical parameters across specimens with approximately similar geometry. Other important sources of uncertainty—such as measurement noise, model-form errors, and geometric variability—were not considered in the current framework. Future work could extend this approach by incorporating these additional sources of uncertainty.

Declaration of competing interest

The author declares that he has no known competing financial interests or personal relationships that could have appeared to influence the work reported in this paper.



Click here to access/download
Supporting File
supportive_file_graphs_set.pdf

Stochastic Calibration of Biological Tissue Biomechanics: Bridging *In-Vitro* Measurements and *In-Silico* Simulations

Mahmut Pekedis^a

^aDepartment of Mechanical Engineering, Ege University, 35040, Bornova, Izmir, 35040, Turkey

Abstract

This study proposes a simple and practical approach based on *in-vitro* measurements and *in-silico* simulations using the likelihood-free Bayesian inference with the finite element method simultaneously for stochastic calibration and uncertainty quantification of the mechanical response of biological materials. We implement the approach for distal, middle, and proximal human Achilles tendon specimens obtained from diabetic patients post-amputation. A wide range of *in-vitro* loading conditions are considered, including one-step and two-step relaxation, as well as incremental cyclic loading tests. *In-silico* simulations are performed for the tendons assuming a fiber-reinforced viscoelastic response, which is modeled separately for the ground matrix and fiber components. Initially, the calibration of the specimen-specific parameters is predicted using Bayesian optimization and the sensitivity of each parameter is evaluated using the Sobol index and random forest. Then, the bounds of these parameters are used as priors, uniformly sampled, and coupled with *in-vitro* data in simulation-based approximate Bayesian computations to calibrate and quantify the uncertainty parameters for three loading cases. The results demonstrate that increasing the number of loading scenarios improves the accuracy of the specimen-specific best-fit parameter set. Furthermore, approximate Bayesian inference shows that *in-silico* simulations using the posterior parameters, can capture the uncertainty bounds of *in-vitro* measurements. This approach provides a useful framework for stochastic calibration of constitutive material model parameters without the need to derive a likelihood function, regardless of the specimen's geometry or loading conditions.

Keywords: *In-vitro* measurements, *in-silico* simulations, biological materials, uncertainty quantification, stochastic material calibration, approximate Bayesian computation, finite element method

1. Introduction

1 *In-silico* mechanical modeling and simulation of biological materials has the potential to facilitate
 2 advancements in every aspect of the medical field. It offers numerous advantages, such as a
 3 promising tool for pre-clinical testing of medical devices, aiding in the diagnosis and evaluation of
 4 targeted treatments for patient-specific applications, and supplementing experimental investigations
 5 when *in-vivo* experiments are not possible [1, 2, 3, 4]. It can also model patient-specific tissue or
 6 organ-level behavior and, more generally, account for variations within a population. One such fac-
 7 tor that significantly influences the *in-silico* simulation outcome is the constitutive material model,
 8 as well as the parameters used in it. The model and its calibrated biomechanical parameters should
 9 accurately reflect and mimic the tissue's behavior. These parameters are typically calibrated using
 10 a non-linear least squares fit of the model to mechanical testing data from experiments such as
 11 tension [5, 6], compression [7], and biaxial testing [8]. For most calibration procedures, the choice of
 12 a constitutive model is assessed by the quality of fit (e.g., R^2 and the value of the root mean square
 13 error RMSE). This technique is efficient and powerful for patient or specimen-specific calibration.

Email address: mahmut.pekedis@ege.edu.tr (Mahmut Pekedis)

14 However, because most biological materials are nonhomogeneous and anisotropic, deploying exper-
15 imental tests using standard mechanical tests may not be enough for mechanical characterization
16 of the tissue. Therefore, calibration of the model parameters directly from the experimental data
17 may not always be possible or relevant. In some studies, the inverse technique is performed to
18 overcome these issues [9, 10]. In brief, the inverse approach is considered as the estimation of input
19 parameters (material properties, geometric features, loading and boundary conditions, etc.) from
20 output observations (displacement, strains, velocity). Once a forward model is created, the input
21 parameters are predicted using experimental observations with an optimization technique. This
22 method is powerful for patient/specimen-specific material calibration when inter-variability is not
23 considered.

24 In addition to inhomogeneous characteristics, biological materials often exhibit intrinsic vari-
25 ability in their biomechanical response when subjected to external loads. The inter-subject or
26 inter-specimen variability and uncertainty in biomechanical properties of these materials are high,
27 which may be influenced by many factors such as the donor’s age, genetics, the tissue’s pathological
28 state, gender, and other specific factors related to the tissue characteristics. For *in-vitro* samples,
29 embalming medium, temperature, humidity, and duration are the additional factors that can affect
30 the biomechanical properties. Oftentimes, *in-silico* model is hindered not only by the incomplete-
31 ness of the theoretical approach but also by uncertainties due to mentioned factors that arise in the
32 experimental observations. Thus, there is an urgent need to ensure that it can capture the intrinsic
33 population of variability and not only be representative of ‘mean’ individuals.

34 Uncertainty can also arise due to a lack of knowledge of the physical model of interest (insufficient
35 initial and boundary conditions), as an addendum to the inherent variation in material properties
36 [11, 12]. However, most of the studies implemented in the field of biomechanics have mainly in-
37 vestigated uncertainties due to variabilities in material properties using the Bayesian framework
38 [13, 14]. In this framework, once the prior distribution of the parameters, in conjunction with a
39 likelihood function, is constructed, the posterior distribution is determined using random sampling
40 methods. There has been much research in the field of brain mechanics [15, 16, 17, 18, 13]. Fur-
41 thermore, several studies have established the utility of Bayesian inference in solid mechanics and
42 soft tissues, addressing both parameter estimation and model selection. For instance, Madireddy
43 et al. [15, 19] presented a Bayesian model selection and calibration framework for hyperelastic soft
44 tissue models. Haughton et al. [20] used Bayesian techniques to quantify uncertainty in microstruc-
45 tural tendon models. Oden et al. [21] and Chiachio et al. [22] implemented Bayesian methods
46 for selecting and validating phenomenological and damage progression models. Rappel et al. [23]
47 provided detailed frameworks to identify the parameters of the elastoplastic material under uncer-
48 tainty. In addition, James Beck and colleagues have applied Bayesian learning to structural health
49 monitoring and inverse problems in mechanics [24, 25, 26, 27]. Furthermore, Babuska et al. [28]
50 presented a Bayesian model comparison approach for metallic fatigue data, while Xue et al. [29] pro-
51 posed sparse Bayesian learning framework for robust damage localization using guided-wave testing.
52 These studies primarily rely on standard Bayesian frameworks that require an explicit likelihood
53 function or surrogate-assisted inference. However, the likelihood function can be difficult or compu-
54 tationally expensive to derive for nonhomogeneous materials under complex biomechanical loading
55 conditions. To overcome these such issues, an approximate Bayesian computation (ABC) approach
56 that does not use the likelihood function has been proposed [30, 31] and implemented recently in
57 some fields including structural health monitoring [32] medical decision making [33] and operation
58 research management [34]. However, the coupling of *in-silico* simulations for stochastic calibration
59 and uncertainty quantification using likelihood-free Bayesian computation in the field of mechanics
60 of biological materials with high inter-specimen variability has been largely unaddressed to date,
61 to the best of our knowledge. The most attractive aspect of this approach is that the likelihood

62 function is not required to be explicitly represented in a closed analytical form. Once an *in-silico*
63 model is built to mimic the *in-vitro* conditions, it directly bypasses the need for explicit likelihood
64 evaluation and relies on comparing the simulated data from the *in-silico* model with experimental
65 observations from the *in-vitro* test. This approach can be implemented in a wide range of *in-vivo*
66 and *in-vitro* applications, ranging from predicting the mechanical characteristics change of tissue
67 due to the risk of pathogenic disease to planning surgical procedures. We note that this study is not
68 targeted to develop or present a constitutive material model for connective tissue, but rather to show
69 how likelihood-free inference can be used directly with the numerical simulator and measurements.
70 Any suggested model can be directly embedded in the simulator.

71 In this work, we suggest a simple approach based on *in-vitro* measurements, *in-silico* simulations,
72 and approximate Bayesian computation for stochastic calibration and uncertainty quantification of
73 material parameters. The paper is structured as follows. First, a specimen-specific calibration
74 procedure using Bayesian optimization is presented. Next, the sensitivity analysis and stochastic
75 calibration steps implemented in ABC are detailed in the following section. Finally, the results
76 obtained from the methodology are presented and summarized, together with some concluding
77 remarks.

78 2. Materials and Methods

79 2.1. *In-vitro* measurements

80 The approach is performed on recently published data of Achilles tendons from diabetic patients
81 who underwent below or above knee amputation [35]. In summary, the tendons were harvested
82 from the proximal end to the insertion of the Achilles tendon at the calcaneus. Their length was
83 about 120 to 130 cm and were partitioned into three equal sections (distal, middle, and proximal
84 site). Then, they were resectioned to form a standard dog bone specimen. The dimensions of each
85 specimen at the measurement site had a gauge length of approximately 10 mm, a width of ~ 8
86 mm and a thickness of ~ 4 mm. Uniaxial displacement-type loading was performed to collect force
87 measurements. First, samples were preloaded at 0.1 MPa to achieve parallel alignment of the fibrils,
88 and then preconditioned for 10 cycles with a strain amplitude of 2% strain at a strain rate of 0.5%
89 s^{-1} . The test protocols were as follows:

- 90 • One-step relaxation: Initiates with a ramp strain of $0.6\% s^{-1}$ followed by a constant strain of
91 4% for a relaxation duration of 200 s (Figure 1a).
- 92 • Two-step relaxation: Two consecutive steps of 2% strain (ramp strain of $0.6\% s^{-1}$) followed
93 by a 200-s relaxation time (Figure 1b).
- 94 • Incremental cyclic: Incremental cyclic loading ranging from a strain amplitude of 2% to 4.25%
95 with an increment of 0.2% strain in each cycle (Figure 1c).

96 Further details of the tests and *in-vitro* measurements are reported in previous work [35]. A typical
97 stress-strain observation of a specimen for three loading scenarios is presented in Figure 1. The force
98 and displacement signals have a sampling rate of 100 Hz. *In-vitro* measurements include 81 datasets
99 (9 specimens \times 3 sites \times 3 test protocols). Each of these data sets consists of three dimensions: the
100 first is time, the second is displacement, and the third is force. The data sets are organized and
101 saved as PYTHON pickle for further serialization processes between *in-vitro* measurements and
102 *in-silico* simulations for sensitivity, optimization and Bayesian inference tasks.

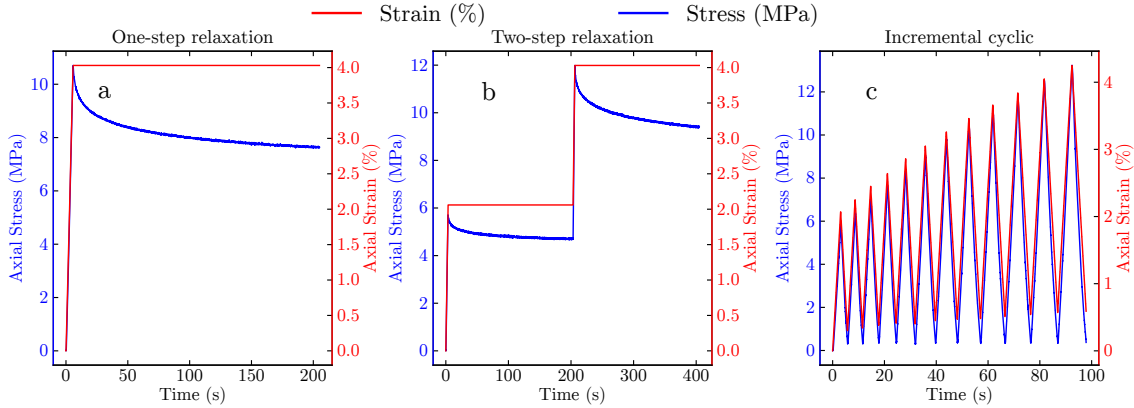


Figure 1: Typical experimental *in-vitro* measurements observed for a specimen. (a) One-step relaxation. (b) Two-step relaxation. (c) Incremental cyclic loading

103 2.2. *Fiber reinforced visco elastic model*

104 Soft biological tissues, such as the Achilles tendon, are collagenous tissues that connect the calf
 105 muscle to the calcaneus. Their primary function is to transmit tensile forces and act as mechanical
 106 dampers. These tissues are primarily composed of water, Type I collagen fibers, and proteoglycans.
 107 They can be viewed as fibrous composites, consisting of a ground matrix embedded with families of
 108 collagen fibers. The tendon is modeled using the fiber-reinforced viscoelastic (FRVE) approach, in
 109 which the solid matrix is divided into a nonfibrillar part representing the proteoglycan matrix and
 110 a fibrillar part representing the collagen fibers. The biomechanical response of these constituents,
 111 which drives the approximate Bayesian computation (ABC), is simulated using the FEBio frame-
 112 work [36]. In this FRVE model, two solid mixtures are considered: the ground matrix, representing
 113 the proteoglycan matrix, and the collagen fibrils, representing the fibers. Viscoelastic effects are
 114 incorporated for both constituents. Specifically, the ground matrix is modeled as a compressible
 115 visco linear elastic material, whereas the collagen fibrils are assumed to be compressible visco non-
 116 linear elastic materials that respond only to tensile loads. The relaxation function for the fibril and
 117 matrix components is given by:

$$G(t) = g_0 + \sum_{i=1}^n g_i e^{-\frac{t}{\tau_i}} \quad (1)$$

118 where t is time, g_i and τ_i are i 'th viscoelastic characteristic coefficients. The strain energy density
 119 function for the fiber component is defined as:

$$\psi_n = \begin{cases} 0, & I_n < 1 \quad (\text{under compression}) \\ \frac{\xi}{\alpha\beta} (\exp [\alpha(I_n - 1)^\beta] - 1), & 1 \leq I_n \leq I_0 \quad (\text{nonlinear toe region}) \\ B(I_n - I_0) - E_f (I_n^{1/2} - I_0^{1/2}) + \frac{\xi}{\alpha\beta} (\exp [\alpha(I_0 - 1)^\beta] - 1), & I_n > I_0 \quad (\text{linear region}) \end{cases} \quad (2)$$

120 where E_f is the fiber modulus in the linear region, α is the coefficient of the exponential term, and
 121 β is the power-law exponent that controls the nonlinearity in the toe region. The scalar quantity
 122 λ_n represents the fiber stretch ratio, defined as the ratio of the current fiber length to its reference
 123 length. The related invariant I_n corresponds to the square of the fiber stretch ratio, $I_n = \lambda_n^2$. A
 124 threshold value $I_0 = \lambda_0^2$ defines the transition from the nonlinear toe region to the linear region of
 125 the material response. The coefficients ξ and B are defined to ensure continuity of the strain energy

126 function:

$$\xi = \frac{E_f(I_0 - 1)^{2-\beta} \exp [-\alpha(I_0 - 1)^\beta]}{4I_0^{3/2} (\beta - 1 + \alpha\beta(I_0 - 1)^\beta)}, \quad (3)$$

127

$$B = E_f \frac{2I_0 \left(\beta - \frac{1}{2} + \alpha\beta(I_0 - 1)^\beta \right) - 1}{4I_0^{3/2} (\beta - 1 + \alpha\beta(I_0 - 1)^\beta)}. \quad (4)$$

128 *In-vitro* measurements showed that λ_0 is approximately 1.01 and assumed to be a fixed parameter.
 129 For this material type, the fiber modulus at the strain origin reduces to zero unless $\beta = 2$. Thus,
 130 we set $\beta = 2$ in the *in-silico* simulation. In summary, the matrix is assumed to exhibit viscoelastic
 131 behavior, while the fiber is modeled as a viscoelastic component that provides tensile reinforcement,
 132 using the **fiber-exp-pow-linear** material model available in FEBio. This approach captures both
 133 the time-dependent behavior and the load-bearing property of the fibers within the composite
 134 tissue. For additional theoretical background, see [36, 37]. The model parameters, their Bayesian
 optimization search ranges, and prior distributions are summarized in Table 1.

Table 1: Parameter space used in Bayesian optimization (BO) and approximate Bayesian computation (ABC) for the three sites.

Constituent	Parameter	Description	Ranges (Min, Max)
Fiber	E_f (MPa)	Fiber modulus	(160, 275)
	a (-)	Exponential argument	(0, 50E3)* and (0, 10E3)**
	g_{1f} (MPa)	1 st viscoelastic characteristic	(0.8, 1)
	g_{2f} (MPa)	2 nd viscoelastic characteristic	(0.8, 2.1)
	g_{3f} (MPa)	3 rd viscoelastic characteristic	(0.8, 2.1)
	τ_{1f} (s)	1 st viscoelastic relaxation	(0.1, 2)
	τ_{2f} (s)	2 nd viscoelastic relaxation	(2, 20)
Ground Matrix	τ_{3f} (s)	3 rd viscoelastic relaxation	(20, 200)
	E_m (MPa)	Elastic modulus	(11, 70)
	g_{1m} (MPa)	1 st viscoelastic characteristic	(0.8, 1.5)
	g_{2m} (MPa)	2 nd viscoelastic characteristic	(0.8, 2.1)
	g_{3m} (MPa)	3 rd viscoelastic characteristic	(0.8, 2.1)
	τ_{1m} (s)	1 st viscoelastic relaxation	(0.1, 2)
	τ_{2m} (s)	2 nd viscoelastic relaxation	(3, 20)
	τ_{3m} (s)	3 rd viscoelastic relaxation	(20, 200)
	v_m (-)	Poisson's ratio	(0, 0.4)

Min and Max values represent the search ranges used in BO.

Min and Max values are also used as uniformly distributed prior ranges for ABC.

*represents α search ranges in BO and, **denotes uniformly distributed prior ranges of α for ABC.

135

136 2.3. *In-silico* simulations

137 Numerical methods such as the finite element method, meshless methods, or the finite volume
 138 method can be used as simulators to bridge the gap between *in-vitro* measurements and Bayesian
 139 computation for stochastic calibration and quantification of uncertainty in the biomechanical re-
 140 sponse of biological materials. Here, we used the finite element method as a simulator. The

141 geometric dimensions of the *in-vitro* sample are approximately $10 \times 8 \times 4$ mm (gauge length \times width
 142 \times thickness). To reduce computational cost, the sample is modeled using a single 3D hexahedral
 143 element, with symmetry imposed in the y -direction by constraining the left face ($u_y(t) = 0$), as
 144 shown in Figure 2. The bottom nodes are constrained vertically ($u_z(t) = 0$), and the top nodes
 145 are displacement-controlled using measured displacements $u_z(t)$, consistent with the *in-vitro* test
 146 protocols. We note that additional *in-silico* outputs, such as the deformation gradient, the strain
 147 distribution, or the direct stress, can also be extracted and used with ABC if the corresponding
 148 measurements are available. Typically, full-field deformation measurements can be collected via
 149 image-based techniques, such as digital image correlation. We believe that higher-dimensional data
 from *in-vitro* observations will lead to more sensitive calibrated parameters.

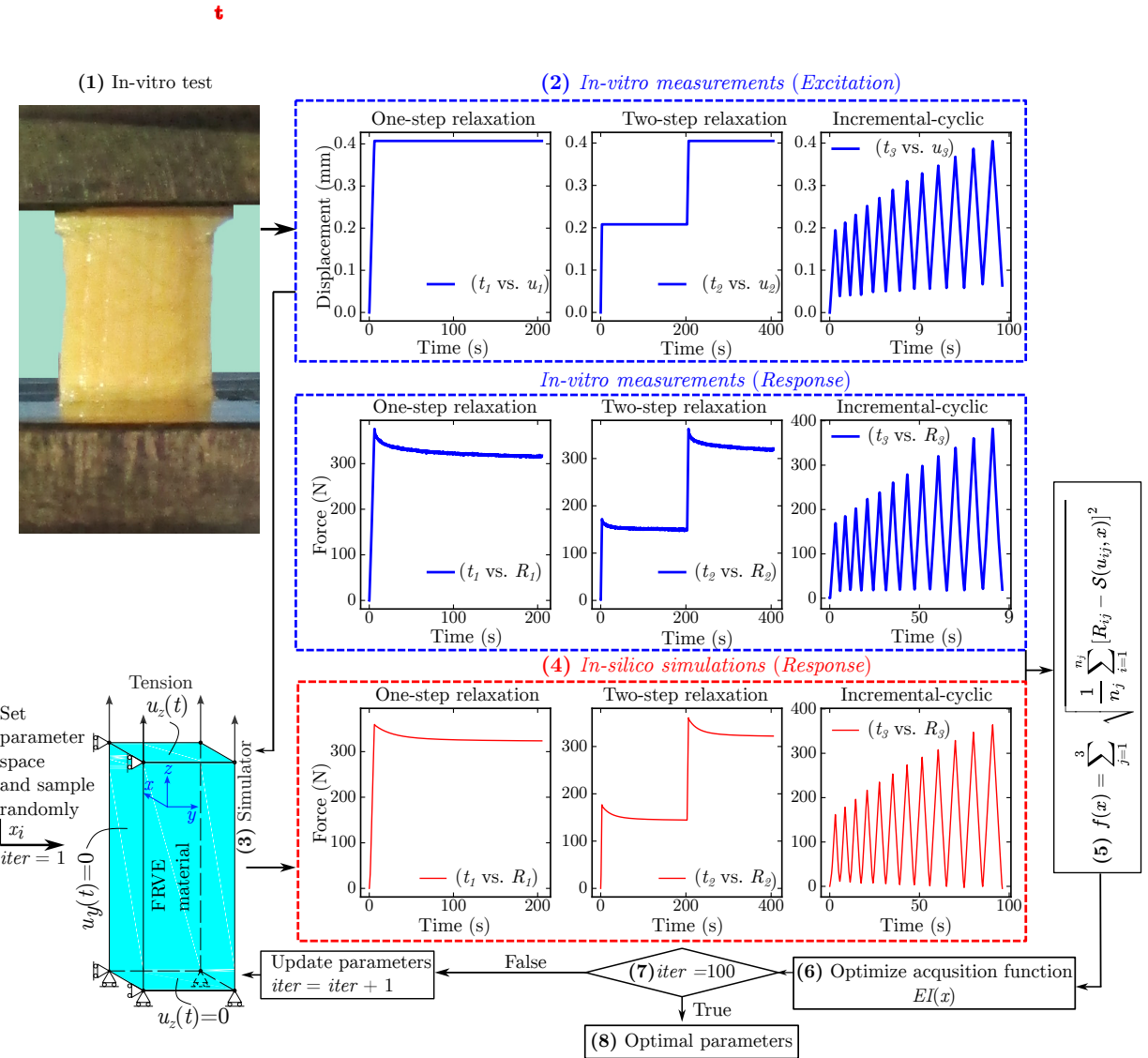


Figure 2: Specimen-specific parameter calibration steps using *in-vitro* measurements, *in-silico* simulations, and Bayesian optimization

151 2.4. Bayesian optimization and sensitivity analysis

152 To determine specimen-specific biomechanical parameters, Bayesian optimization (BO) is imple-
 153 mented using `scikit-optimize` library. BO was selected primarily due to the high computational
 154 cost of finite element simulations involved in evaluating the objective function $f(x)$. Each evaluation
 155 requires solving a full-scale FE model, making traditional methods such as grid search or evolution-
 156 ary algorithms computationally impractical. Beyond efficient parameter calibration, BO also served
 157 two purposes in this study: (i) to inform the parameter ranges used as priors in the ABC-based
 158 uncertainty quantification framework, and (ii) to compare frequentist estimates obtained from BO
 159 with probabilistic posteriors derived from ABC, thus enabling a direct comparison between deter-
 160 ministic and stochastic inference approaches. BO is an iterative framework focused on optimizing
 161 an expensive and unknown objective function $f(x)$, where $x \in \mathbb{R}^d$ is a vector of d parameters. The
 162 goal is to solve

$$\mathbf{x}^* = \arg \min_{\mathbf{x} \in \mathcal{A}} f(\mathbf{x}) \quad (5)$$

163 where \mathcal{A} is the search space. The gradient information is unavailable for $f(x)$ and is considered a
 164 "black box" function. The core of BO is based on constructing a probabilistic surrogate model, a
 165 Gaussian process (GP) to approximate $f(x)$. It models the unknown objective function $f(x)$ by
 166 providing a posterior distribution given the observed data. With its simplest form, the resulting
 167 prior of GP is written as:

$$f(x) \sim \mathcal{GP}(\mu(x), k(x, x')) \quad (6)$$

168 where $\mu(x)$ is the mean function, showing the prior belief about the objective function and $k(x, x')$
 169 is the covariance (or kernel) function. In this study, the surrogate model was built using a Gaussian
 170 Process (GP) with a Matérn kernel, as provided by the `scikit-optimize` library. An anisotropic
 171 kernel was used, allowing a separate length-scale to be estimated for each parameter dimension. The
 172 optimization process was initialized using random sampling strategy. Once building the surrogate
 173 model, Bayesian optimization selects the next point x_{next} to evaluate by maximizing an *acquisition*
 174 *function*. A common acquisition function used in `scikit-optimize` is *Expected Improvement* (EI)
 175 and defined as:

$$\text{EI}(x) = \mathbb{E} [\max(f^* - f(x), 0)] \quad (7)$$

176 where f^* is the current best observed value of $f(x)$. The $f(x)$ function at any x point is normally
 177 distributed with mean $\mu(x)$ and variance $\sigma^2(x)$, and the improvement is modeled as:

$$\text{EI}(x) = (\mu(x) - f^*)\Phi\left(\frac{\mu(x) - f^*}{\sigma(x)}\right) + \sigma(x)\phi\left(\frac{\mu(x) - f^*}{\sigma(x)}\right) \quad (8)$$

178 where $\Phi(\cdot)$ is the cumulative distribution function (CDF) and $\phi(\cdot)$ is the probability density func-
 179 tion (PDF) of the standard normal distribution, respectively. This acquisition function seeks regions
 180 where the model predicts the largest improvement over the current best value. To find the next
 181 sampling point x_{next} , the acquisition function $\text{EI}(x)$ is maximized. Once a new sample x_{next} is se-
 182 lected and the objective function $f(x_{\text{next}})$ is evaluated, the surrogate model (the Gaussian Process)
 183 is updated. The process continues until a stopping criterion is met. Further details of BO are doc-
 184 umented in literature [38]. We empirically observed that a fixed stopping criterion of 100 iterations
 185 provided sufficient convergence for the calibration of specimen-specific parameters. While adaptive
 186 criteria, such as convergence thresholds, may be more theoretically grounded, we found that using a
 187 fixed number of iterations ensured predictable computational costs and produced consistent results
 188 across specimens in our setting. In preliminary tests, threshold-based stopping led to extended
 189 runtimes without significant gains in accuracy. Therefore, we adopted a fixed-iteration approach

190 for practical and computational efficiency. The objective function to be minimized is defined as the
 191 summation of the root mean square error (RMSE) between experimental (*in-vitro*) and numerical
 192 (*in-silico*) total reaction force values for the three loading scenarios. It is given by:

$$f(x) = \sum_{j=1}^3 \sqrt{\frac{1}{n_j} \sum_{i=1}^{n_j} [R_{ij} - 2\mathcal{S}(u_{ij}, x)]^2} \quad (9)$$

193 where R_{ij} and $\mathcal{S}(u_{ij}, x)$ are the experimental and numerical reaction forces, respectively, for the
 194 parameter set x at displacement u_{ij} , and data point i . The term n_j denotes the number of data
 195 points for test loading j , where $j = 1$ corresponds to the one-step relaxation, $j = 2$ to the two-step
 196 relaxation, and $j = 3$ to the incremental cyclic loading scenario. The factor of 2 in the equation
 197 arises from the symmetric boundary conditions modeled in the finite element (FE) simulation.
 198 Simply, the (R_{ij}, u_{ij}) are *in-vitro* observation pairs, and $\mathcal{S}(u_{ij}, x)$ is the unknown force function
 199 that extracts the corresponding data from the FE simulator. The BO tries to find the model
 200 parameters x that minimize the function $f(x)$ by repeatedly evaluating the function $EI(x)$, which
 201 calls the simulator (FEBio) to solve the black-box problem. The parameter search ranges used
 202 during BO are given in Table 1, and the initial search ranges for these parameters are predicted
 203 as follows. First, the viscoelastic characteristics g_i and τ_i are estimated by fitting on some trial
 204 one-step relaxation measurements using the Levenberg–Marquardt method. Then, the bounds of
 205 the estimated parameters are extended and used as search ranges for BO. Similar search ranges are
 206 considered for the fiber and matrix components. For the approximate prediction of the modulus,
 207 we initially evaluated it by analyzing the linear region of a typical incremental cyclic test loading
 208 measurement and found that the modulus of elasticity for the composite tendon (matrix + fiber)
 209 is around 350 MP. Although, to the best of our knowledge, no study has experimentally quantified
 210 the elastic modulus of the fiber and elastic component in the human Achilles tendon separately, it
 211 has been stated in some rat studies that the fiber-to-matrix ratio is between 5 and 10 [39, 40, 41].

212 Sensitivity and feature importance analyses are performed to investigate the influence of each
 213 parameter on the FRVE model for each test loading scenario. Feature importance is determined
 214 using the random forest algorithm implemented in `scikit-learn`, which is based on impurity re-
 215 duction. The importance of a feature is computed as the total reduction of the criterion observed
 216 by the feature, known as the Gini importance [42]. The importance of a feature $I(x_i)$ is given by:

$$I(x_i) = \frac{1}{n_t} \sum_1^{n_t} \sum_{s \in S_t(x_i)} \Delta I_s \quad (10)$$

217 where n_t is the number of trees in the forest, $S_t(x_i)$ is the set of all splits for the feature x_i in the tree
 218 t , and ΔI_s is the decrease in the splitting criteria at split s . The final importance values are then
 219 normalized to 100 over all features. More details on the random forest algorithm are documented
 220 in the literature [42].

221 As an addendum to the feature importance analysis, we implemented Sobol sensitivity analysis
 222 to investigate the sensitivity of the input parameters on the model output using `salib` [43]. It is
 223 a variance-based approach to quantify the parameter's sensitivity as well as their contribution to
 224 the model. Basically, it decomposes the total variance of the output Y into contributions that are
 225 attributable to input parameters and their interactions. Let us assume that $Y = f(X_1, X_2, \dots, X_d)$
 226 represents the model output as a function of d input parameters X_1, X_2, \dots, X_d . The total variance

227 of Y is given by:

$$V = \text{Var}(Y) = \int (f(\mathbf{X}) - E[Y])^2 p(\mathbf{X}) d\mathbf{X} \quad (11)$$

228 where $p(\mathbf{X})$ shows the joint probability density function for the inputs. The variance can be decom-
229 posed as:

$$V = \sum_{i=1}^d V_i + \sum_{1 \leq i < j \leq d} V_{ij} + \cdots + V_{12\dots d} \quad (12)$$

230 where $V_i = \text{Var}(E[Y | X_i])$ represents the main effect of input X_i , and $V_{ij} = \text{Var}(E[Y | X_i, X_j]) -$
231 $V_i - V_j$ shows the interaction effect between X_i and X_j . Higher-order terms denote interactions
232 between more input parameters. The Sobol indices are dimensionless quantities that measure the
233 relative contribution of each term to the total variance. The first-order sensitivity index is given
234 by:

$$S_i = \frac{V_i}{V}. \quad (13)$$

235 The first-order index shows the proportion of variance that is attributed to X_i . Total-order sensi-
236 tivity index is given by:

$$S_{T_i} = 1 - \frac{V_{\sim i}}{V} \quad (14)$$

237 where $V_{\sim i}$ is the variance of the output excluding X_i . The total-order index accounts for both
238 the main effect and all interaction effects involving X_i . The interaction terms (e.g., S_{ij}) can be
239 calculated similarly by dividing the corresponding variance term by the total variance. However,
240 the sensitivity due to interaction is not covered in this study. We implemented Saltelli sampling to
241 create the parameter space of 20,000 points for each of the 16 input parameters of the FRVE model.
242 In our Saltelli-based Sobol sensitivity analysis, we employed uniform distributions over the parame-
243 ter ranges as defined in Table 1. These ranges were initially informed by the results of the Bayesian
244 Optimization (BO). While using uniform priors over these ranges enables non-informative sampling
245 and is a common practice in variance-based sensitivity analysis, we acknowledge the limitations
246 of this approach. Specifically, this choice may not capture the true posterior distributions of the
247 parameters — particularly if the underlying parameter space is multimodal or exhibits strong cor-
248 relations. Future work could involve using posterior-informed distributions to improve the fidelity
249 of sensitivity estimates.

250 To ensure stable and theoretically consistent sensitivity index computation, we implemented a
251 normalization strategy for all 16 input parameters. Each parameter was scaled to the [0,1] inter-
252 val based on its empirical minimum and maximum values across the dataset. This step not only
253 facilitates variance-based decomposition but also helps avoid scale-related instabilities. The model
254 output used for Sobol analysis was the total error function defined in Eq. 9 which aggregates dis-
255 crepancies across three experimental loading scenarios. During our initial analysis, we observed that
256 the sum of first-order Sobol indices occasionally exceeded 1, which violates theoretical expectations
257 for additive variance decomposition. We identified that this issue was caused by non-smooth be-
258 havior in the output space. To address this, we employed a surrogate modeling strategy using a
259 nearest-neighbor interpolation method. Specifically, Saltelli-generated samples were projected into
260 the empirical parameter space by finding the closest real data points in a normalized feature space.
261 The associated output values from these matched samples were then used for computing Sobol
262 indices. The use of surrogate modeling is a standard remedy for non-smooth or computationally
263 expensive models in global sensitivity analysis and has been recommended in several studies [44, 45].
264 Additional details on the Sobol sensitivity analysis are reported in the previous study [46].

265 *2.5. Approximate Bayesian Computation*

266 Although the standard Bayesian framework allows for updating prior beliefs about parameters
 267 based on the likelihood of the data given those parameters, evaluating the likelihood $P(\mathbf{y}_{\text{obs}}|\boldsymbol{\theta})$ is
 268 often infeasible, but the model can generate synthetic data \mathbf{y}_{sim} given parameters $\boldsymbol{\theta}$. In general,
 269 Bayesian inference provides a principled framework for quantifying uncertainty in model parameters
 270 by combining prior knowledge with evidence from observed data through the likelihood function.
 271 However, for many nonlinear models, deriving an analytical or tractable likelihood function is diffi-
 272 cult or impossible. Here, we implemented likelihood-free approximate Bayesian computation (ABC)
 273 for stochastic calibration and uncertainty quantification of posterior parameters using PyABC [31].
 274 The framework is based on an executable “black-box” forward process model that simulates data
 275 using given model parameters [47, 48]. In ABC, the computation of the likelihood is replaced by
 276 the comparison between observed (*in-vitro* measurements) \mathbf{y}_{obs} and simulated data (*in-silico* sim-
 277 ulations) \mathbf{y}_{sim} . Given the prior distribution of $P(\boldsymbol{\theta})$ of parameters $\boldsymbol{\theta}$, the target is to approximate
 278 the posterior distribution $P(\boldsymbol{\theta}|\mathbf{y}_{\text{obs}})$ given observed data \mathbf{y}_{obs} , a model $f(\mathbf{y}_{\text{sim}}|\boldsymbol{\theta})$, and a prior dis-
 279 tribution $P(\boldsymbol{\theta})$. Typically, it is based on generating simulated data \mathbf{y}_{sim} for parameters $\boldsymbol{\theta}$ drawn
 280 from the prior distribution and retaining parameters for which \mathbf{y}_{sim} is sufficiently close to \mathbf{y}_{obs} . The
 281 posterior is approximated as:

$$P(\boldsymbol{\theta}|\mathbf{y}_{\text{obs}}) \approx P(\boldsymbol{\theta}) \cdot \mathbb{I}(d(\mathbf{y}_{\text{obs}}, \mathbf{y}_{\text{sim}}) \leq \epsilon) \quad (15)$$

282 where $d(\mathbf{y}_{\text{obs}}, \mathbf{y}_{\text{sim}})$ is a distance metric, ϵ is a tolerance threshold, and $\mathbb{I}(\cdot)$ is an indicator function
 283 that equals 1 when the condition is satisfied $d(\mathbf{y}_{\text{obs}}, \mathbf{y}_{\text{sim}}) \leq \epsilon$ and 0 otherwise $d(\mathbf{y}_{\text{obs}}, \mathbf{y}_{\text{sim}}) \geq \epsilon$. The
 284 output of the algorithm is a sample set of parameters from the distribution $P(\boldsymbol{\theta}|d(\mathbf{y}_{\text{obs}}, \mathbf{y}_{\text{sim}}) \leq \epsilon)$.
 285 Direct ABC implementation can be inefficient, particularly for small ϵ , as it reduces the number of
 286 accepted parameters. To overcome this, pyABC performs a Sequential Monte Carlo (SMC) tech-
 287 nique that progressively refines the posterior estimation. It facilitates robust and efficient inference
 288 for a broad spectrum of applications. Further details of ABC model are documented in previous
 289 studies [30].

290 In this study, the prior distributions for the parameters are defined based on a uniform dis-
 291 tribution (Table 1). We note that these priors were informed by initial exploratory analyses and
 292 preliminary specimen-specific calibrations using Bayesian optimization (BO). While this approach
 293 improves sampling efficiency by focusing on physiologically plausible ranges, it does not constitute a
 294 strictly prior-knowledge-based prior in the classical Bayesian sense. The distance between observed
 295 and simulated data is computed using the Euclidean distance (L2) metric. To refine the parameter
 296 estimates, the ϵ tolerance was adaptively adjusted in the ABC SMC process. The initial tolerance
 297 threshold of ϵ is set as 0.3. We note that we selected these options by running some trials and
 298 focusing on where the simulated data \mathbf{y}_{sim} most closely matched the observed data \mathbf{y}_{obs} . While our
 299 current implementation treats ϵ as a fixed threshold that is adaptively decreased within the Sequen-
 300 tial Monte Carlo (SMC) procedure of PyABC, future work could involve treating this tolerance as a
 301 latent variable and inferring it jointly with the model parameters to better reflect observations.

302 *2.6. Implementation procedures*

303 The implementation begins with specimen-specific parameter calibration to determine the ap-
 304 proximate values of the FRVE parameter set using an optimization technique. We employed
 305 Bayesian Optimization (BO), and the procedures and stages of its implementation are illustrated
 306 in Figure 2, where the numbers indicate data processing steps. Initially, *in-vitro* test samples are
 307 harvested and re-sectioned (1). Then in vitro test loading protocols are applied and their mea-
 308 surements are acquired, categorized, and saved as a serialized dataset file (2). As a preliminary

study, we chose a simple uniaxial tensile test for the three test loading scenarios. For each test, the reaction force $R(t)$ is obtained as a function of displacement $u(t)$. This process is applied to all samples. Next, the search space is defined, and the objective function is formulated (3). *In-silico* simulations using the finite element method are performed to obtain time vs. reaction force values (4). The objective function is computed as the difference between *in-silico* and *in-vitro* reaction force observations (5). Once the objective function is minimized in the current step, the next target is to optimize the acquisition function, balancing exploration and exploitation (6-7). The model is then updated by incorporating a new observation and retraining the surrogate model. Finally, steps 3-7 are iterated until the stopping criteria are met (8). To reduce computational time, we set the stopping criterion at 100 iterations, as this was sufficient for calibrating specimen-specific parameters. The implementation of *in-vitro* measurements, coupled with *in-silico* simulation and ABC, resembles the BO stages at the pre-processing steps. However, the main difference is that instead of evaluating specimen-specific observations, ABC includes all specimens' measurements, allowing for the stochastic calibration of parameters, including uncertainty. The implementation procedure and sequence of steps illustrated in Figure 3 are as follows:

1. *In-vitro* test samples are harvested and re-sectioned into an appropriate shape for the biomechanical test. A higher number of samples allows for better quantification.
2. *In-vitro* biomechanical tests are performed to obtain output observations. Here, the resulting reaction forces $R(t)$ are referred to as \mathbf{y}_{obs} . As an addendum to the one-step and two-step relaxation loadings, we include only single-cycle observations (loading-unloading) from the incremental cyclic test during ABC inference.
3. The importance and sensitivity of each parameter are determined using the Random Forest and Sobol methods. Once the minimum and maximum bounds obtained from BO across all samples are determined, these wide bounds are used as priors in ABC. Initially, parameters $\boldsymbol{\theta}$ are drawn from the prior uniform distribution as: $\boldsymbol{\theta} \sim P(\boldsymbol{\theta})$.
4. The next step is to perform forward simulations to drive ABC. We implemented FEBio as the simulator and created a template that includes the FRVE material model and boundary conditions that mimic the experiment. FEBio input files (.feb) are xml type files, and we used the `jinja` package to create the FEBio input template file and serialize the data between ABC and the simulator. Once ABC determines the input parameter set $\boldsymbol{\theta}$, it is passed directly to this simulator template, and the FEBio simulator generates simulated data $f(\mathbf{y}|\boldsymbol{\theta})$ using $\boldsymbol{\theta}$ as: $\mathbf{y}_{\text{sim}} \sim f(\mathbf{y}|\boldsymbol{\theta})$.
5. The distance between the observed and simulated data is computed as: $d = d(\mathbf{y}_{\text{obs}}, \mathbf{y}_{\text{sim}})$, where $d(\cdot)$ is a Euclidean distance metric.
6. The parameter $\boldsymbol{\theta}$ is retained if the distance satisfies: $d \leq \epsilon$; otherwise, return to step 4.
7. The joint plots of the posterior parameters are visualized, and the lower, mean and upper bounds, as well as the confidence interval 95% of the inferred simulation \mathbf{y}_{sim} , are plotted.

3. Results

3.1. Bayesian optimization

We first performed specimen-specific parameter calibration using Bayesian optimization (BO), and the results observed for a typical specimen are represented in Figures 4, 5, 6, and 7. Figure 4 shows that the minimum $f(x)$ function converges rapidly, even with only a few initial iterations. This characteristic makes BO popular in machine learning for hyperparameter optimization, where the learning algorithm is treated as a black-box function. Consider the convergence plot given in

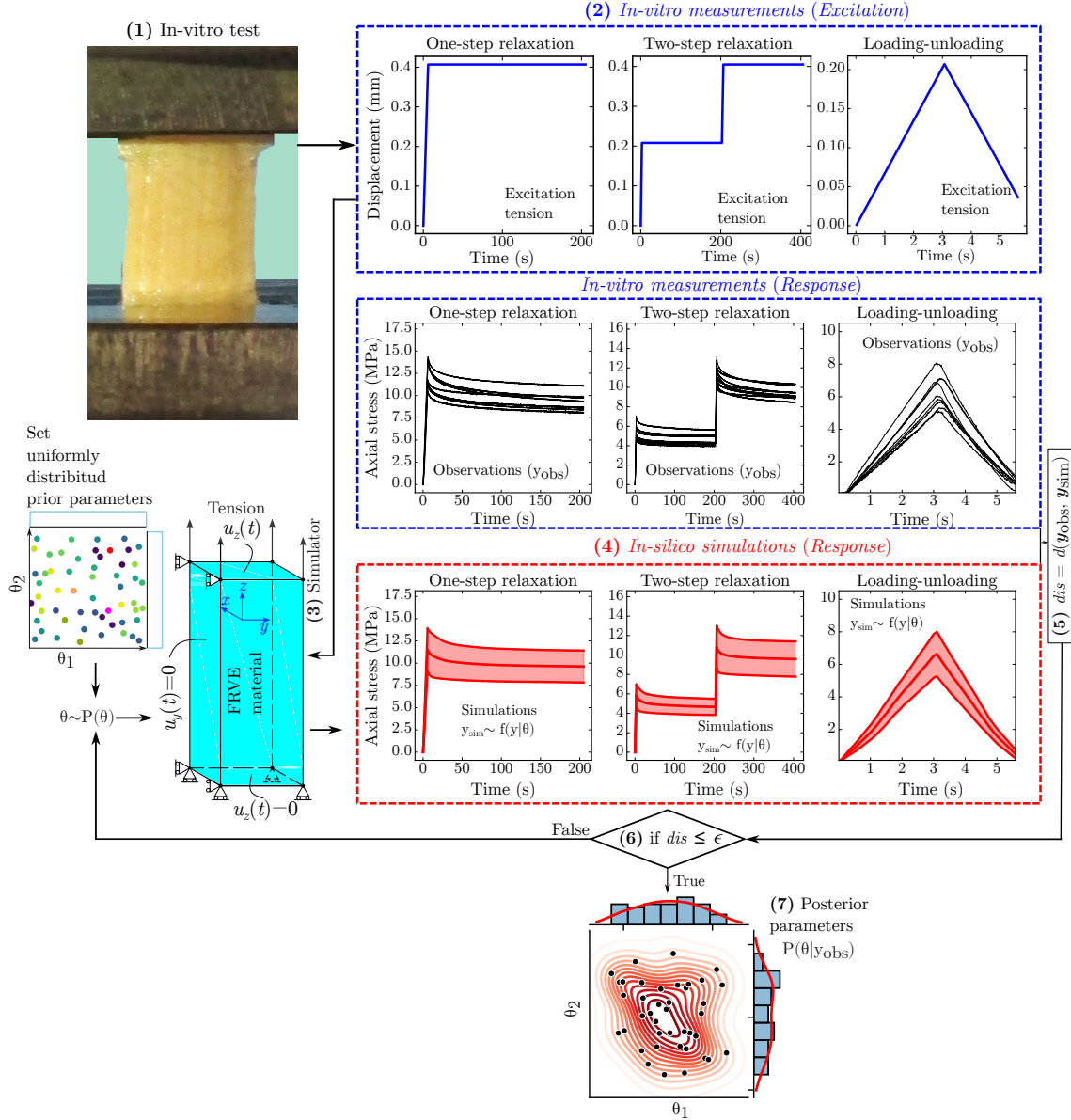


Figure 3: Stochastic parameter calibration steps using *in-vitro* measurements, *in-silico* simulations and approximate Bayesian computation

353 Figure 4; although the initial minimum value $f(x)$ is 65 N, after 100 iterations (or function calls),
 354 it decreases to less than 20 N. In addition, Figure 5 presents the *in-vitro* measurements obtained
 355 from experiments and the *in-silico* observations generated using optimized FRVE parameter sets
 356 in BO. Here, we note that the terms ‘ground truth’, ‘*in-vitro* measurements’, and ‘experimental
 357 observations’ are often used interchangeably to convey a similar meaning. Furthermore, ‘*in-silico*
 358 simulation’, ‘black-box simulator’, and ‘numerical observations’ are also often used interchangeably
 359 to refer to a similar meaning. Figure 5 shows that the minimum $f(x)$ values of the objective
 360 function, determined by incremental cyclic loading test measurements in one step, two steps, and
 361 incremental steps, are 5.693 N, 3.871 N, and 13.232 N, respectively. These results show that the
 362 FRVE model can capture the mechanical response of the tendon.

363 We performed the BO process for 100 calls of the black-box simulator, and the parameter sensi-
 364 tivity can probably be improved once the iteration number is increased. However, this can increase
 365 computational time, and we have not focused on characterizing the parameters with a high rank of
 366 sensitivity. The target of using BO is to determine how the specimen-specific parameters vary across
 367 specimens and to use these parameters to predict the priors for ABC inference. We present some
 368 parameters for matrix and fiber constituent pairs that were sampled during BO updating as scatter
 369 (Figure 6) and contour (Figure 7) plots to visualize where they are mainly clustered. For example,
 370 consider the sample points of E_m and E_f ; the elastic modulus of the matrix and fiber components is
 371 predominantly updated around 60 MPa and 240 MPa, respectively. The remaining parameters for a
 372 typical specimen-specific calibration are given as additional figures (See Supplementary Figure S1
 373 and S2). We then automated the process to characterize the remaining 26 samples, and the overall
 374 results are given in Table 2. These results suggest that inter-subject or inter-specimen variability
 375 and uncertainty in the biomechanical properties of these materials are high.

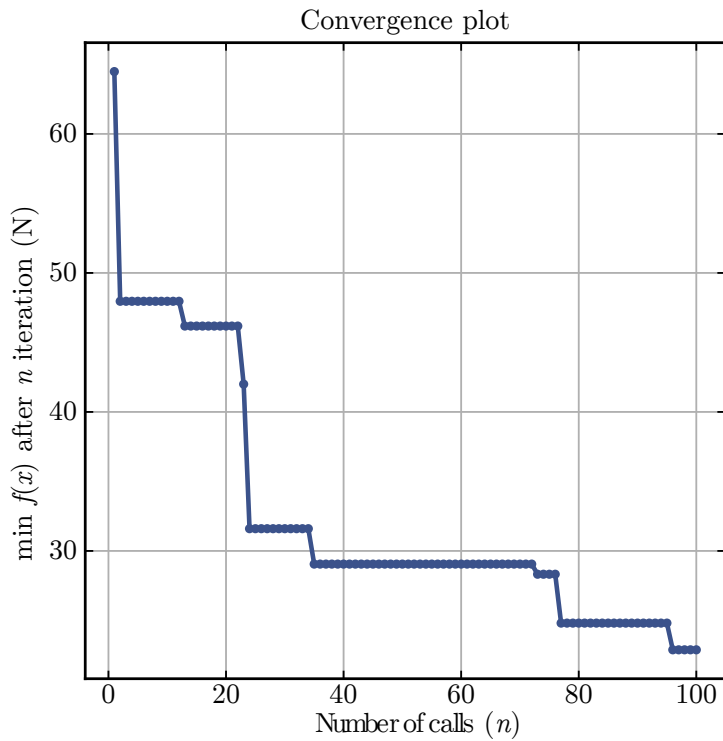


Figure 4: Typical convergence plot of a specimen during Bayesian optimization

376 For the clinical aspect, correlation analysis between micro-scale matrix and fiber parameters
 377 calibrated via BO can also be performed. Here, to account for dependency due to repeated ob-
 378 servations for the same patient's specimen harvested from distal, middle, and proximal sites, we
 379 used the `rm_corr()` repeated measures correlation function from the Pingouin statistical package.
 380 Repeated measures reveal that the most significant correlations are observed between τ_{3m} and τ_{1f}
 381 ($r = 0.8$), g_{3m} and g_{3f} ($r = 0.71$), τ_{2m} and τ_{1f} ($r = 0.69$), g_{2m} and τ_{1f} ($r = 0.65$), g_{2m} and g_{3f} (r
 382 = 0.64), while the only negative significant correlation exists between E_m and τ_{1f} ($r = 0.48$) ($p <$
 383 0.05) (Figure 8).

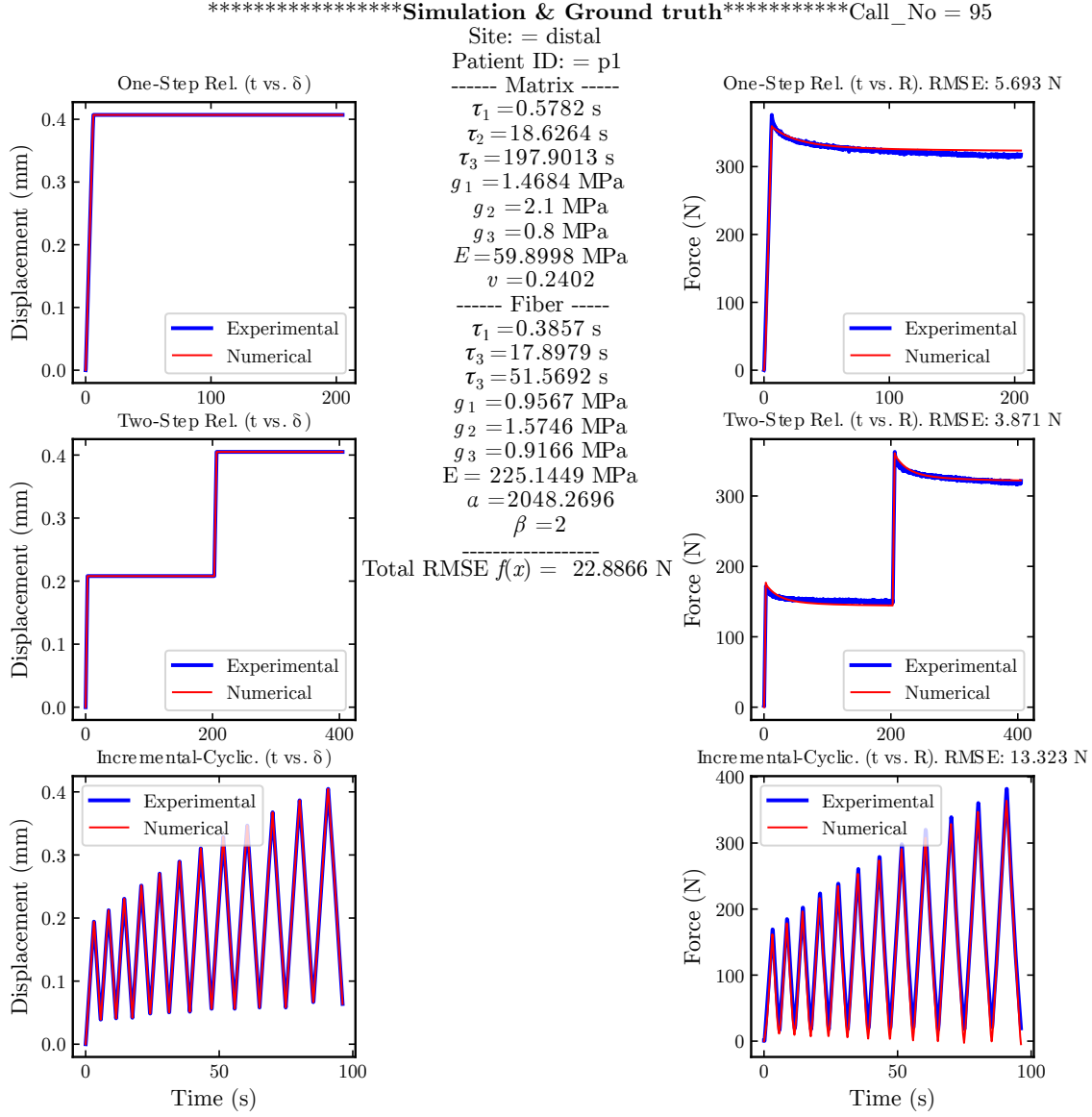


Figure 5: *In-vitro* (ground truth) and *in-silico* (simulation) observations of a typical sample with parameters tuned with Bayesian optimization.

384 3.2. Sensitivity analysis

385 To determine the influence of each parameter on the objective function of FRVE model param-
386 eters, we investigate the percentage importance of the parameters using random forest and their
387 sensitivity using Sobol. Here, we use the error function observations $\min f(x)$ given in Eq. 9 as
388 outputs during sensitivity analysis and importance identification. The results of the random forest
389 for a typical specimen in three loading conditions are represented in Figure 9. As expected, the
390 elastic modulus of the fiber E_f , the exponential coefficient α_f , and the elastic modulus of the ma-
391 trix E_m have the highest feature importance. Interestingly, the viscoelastic characteristics g_{im} and
392 relaxation time coefficients τ_{im} of the ground matrix at the i th Prony order are more important
393 than the fiber's parameters for the combined three-loading $\min f(x)$ function.

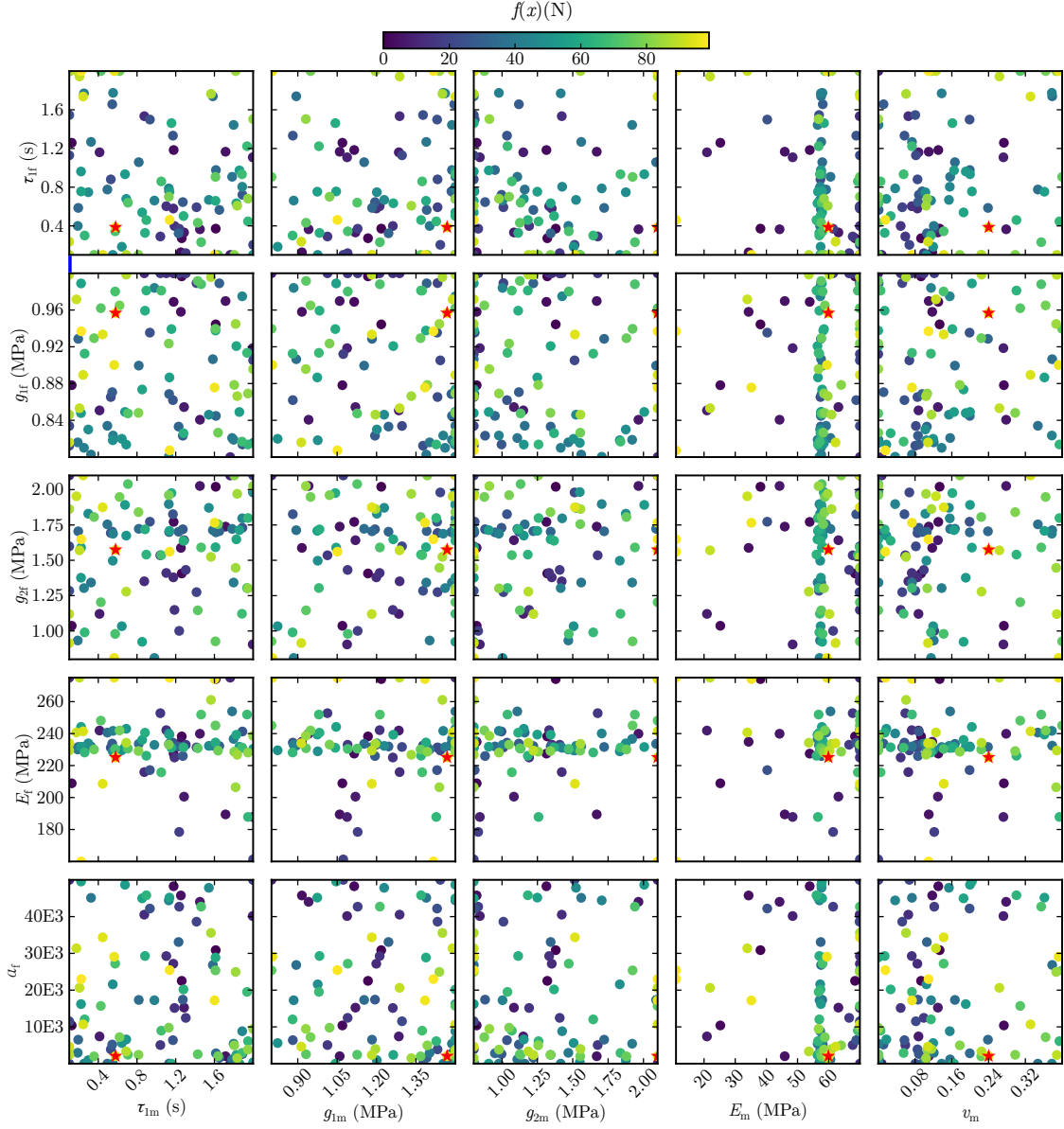


Figure 6: Visualization of the sample points for some parameters of a typical specimen during Bayesian optimization. The red star indicates the best-found parameters.)

394 For Sobol's sensitivity analysis, the parameter space is created using Saltelli sampling. We
 395 generate 20,000 input sampling sets, each consisting of 16 parameters (8 for the ground matrix and
 396 8 for the fiber), and collect the output $\min f(x)$ observations. Similar to the results obtained from
 397 the random forest analysis, E_f , E_m , and α_f are identified as the most sensitive parameters in the
 398 model. The total and first-order sensitivity indices for these parameters are presented in Figure 10.
 399 Based on the total-order index scores, the three most sensitive parameters, in descending order, are:
 400 E_f (0.7325), E_m (0.4905), and α_f (0.3587).

401 3.3. Approximate Bayesian computation

402 We presented specimen-specific parameter identification results in the previous section and ob-
 403 served that the variability in mechanical parameters across samples is high, potentially influenced

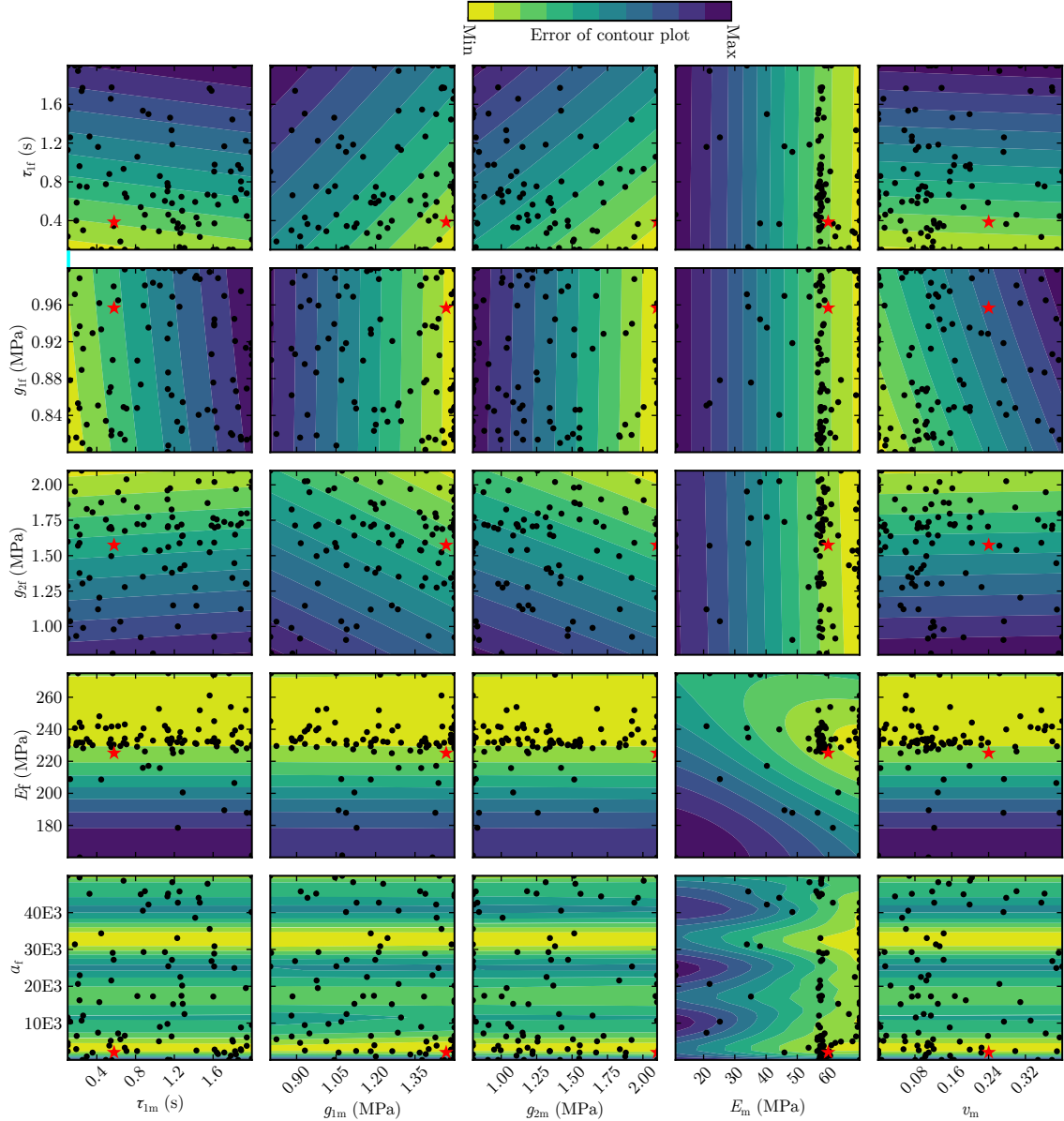


Figure 7: The influence of each search space on the objective function for some parameters observed in a typical specimen during Bayesian optimization. The red star indicates the best-found parameters

404 by factors such as donor age, genetics, tissue pathology, gender, and other sample-specific charac-
 405 teristics. To determine the uncertainty in these parameters and stochastically calibrate them, we
 406 implement likelihood-free inference in a probabilistic framework. The ABC inference is initiated
 407 with a tolerance threshold of $\epsilon = 0.3$, selected empirically to allow for sufficient sampling diversity
 408 in the initial generation. This threshold is adaptively updated by the ABC-SMC algorithm in sub-
 409 sequent populations, progressively tightening the acceptance criterion around the observed data.
 410 In each generation, 40 accepted sample sets are retained. The inferred parameters for the distal,
 411 middle, and proximal sites are given in Table 3. Consider E_f at the distal site: the mean is 216.2
 412 MPa, and the 95% HDI bounds are 164.6 MPa and 267.8 MPa.

413 We have visualized the posterior joint distributions to investigate the relationships, correlations,

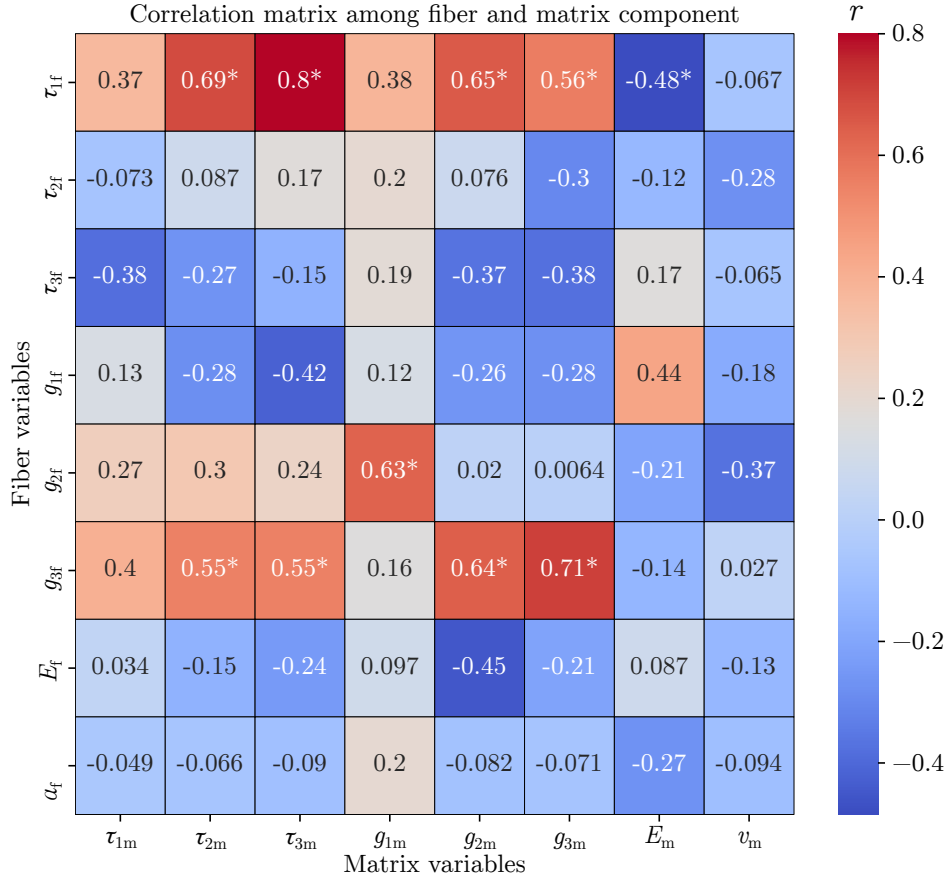


Figure 8: Correlation levels between matrix and fiber variables. *Repeated measures correlation coefficient (r) is significant at the $p < 0.05$ level

and uncertainty between the parameters after updating beliefs based on *in vitro* measurement observations. Some parameter pairs plotted for the matrix and fiber components, as well as their distributions for the distal site, are shown in Figure 11. Consider g_1 : there is a significant negative correlation between the matrix and the fiber component ($r = -0.37$, $p < 0.05$). However, the remaining parameters shown in Figure 11 for the matrix (τ_{1m} , g_{2m} , E_m , v_m) and the fiber (τ_{1f} , g_{1f} , g_{2f} , α_f) are not significantly correlated. The joint posterior plots inferred for 16 parameters for three sites are given in Supplementary Figures S3–S5. Once the calibration of the parameters is complete and their uncertain ranges for the highest density interval (HDI) 95% are inferred, the next step is to investigate how well the simulated data from the posterior $f(y_{sim}|\theta)$ can capture the uncertainties of *in vitro* observations y_{obs} . We perform forward simulations based on posterior parameters (θ) for two cases. In the first case, we performed three simulations: one based on the mean and the other two based on the low and high bounds of θ given in Table 3. We then collected observations from y_{sim} . The inferred observation band is shown in cyan, and its bounds are represented in blue in Figure 12. In the second case, we performed 40 simulations, each corresponding to a single posterior parameter set, and then computed the 95% confidence interval (CI) of the 40 y_{sim} observations. The observation band for the 95% CI and its bounds are represented in red (Figure 12). The observation band for the 95% CI and its bounds are represented in red (Figure 12). The results obtained in both cases demonstrate that the stochastically calibrated model parameters can capture the uncertainty band of *in vitro* measurements (y_{obs}). However, to characterize and simulate the soft tissue response

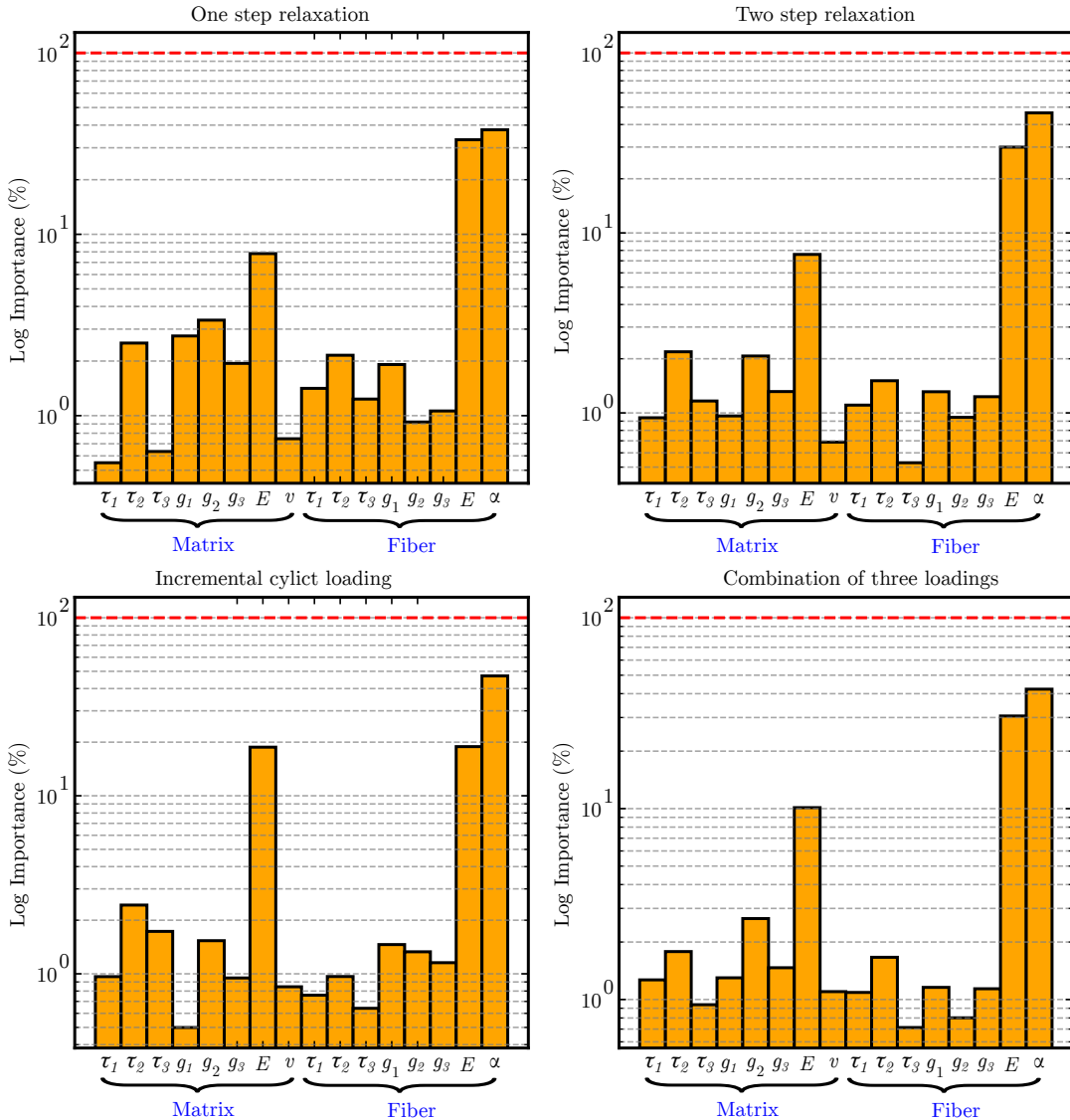


Figure 9: Variables feature importance using Random forest

under extreme uncertainty, it is preferable to use the 95% HDI bound of θ , as demonstrated in case 1.

In some clinical biomechanical studies, it may be necessary to compare the data obtained from different groups. This is usually carried out by applying parametric or non-parametric statistical tests to the results. This approach is effective within a frequentist framework. Although this study does not directly investigate the differences between the three sites, we performed unsupervised machine learning to determine whether the probabilistic data of the groups are clustered and separated. Here, we primarily used principal component analysis (PCA) and receiver operating characteristic (ROC) curves to investigate whether data from different groups could be effectively distinguished. Prior to PCA, we standardized the posteriors θ as $\frac{\theta - \mu}{\sigma}$, where μ is the mean and σ is the standard deviation. Then, we processed 40 parameters with a 16-dimensional posterior parameter set through PCA to reduce them to a single-dimensional component using the **scikit-learn**

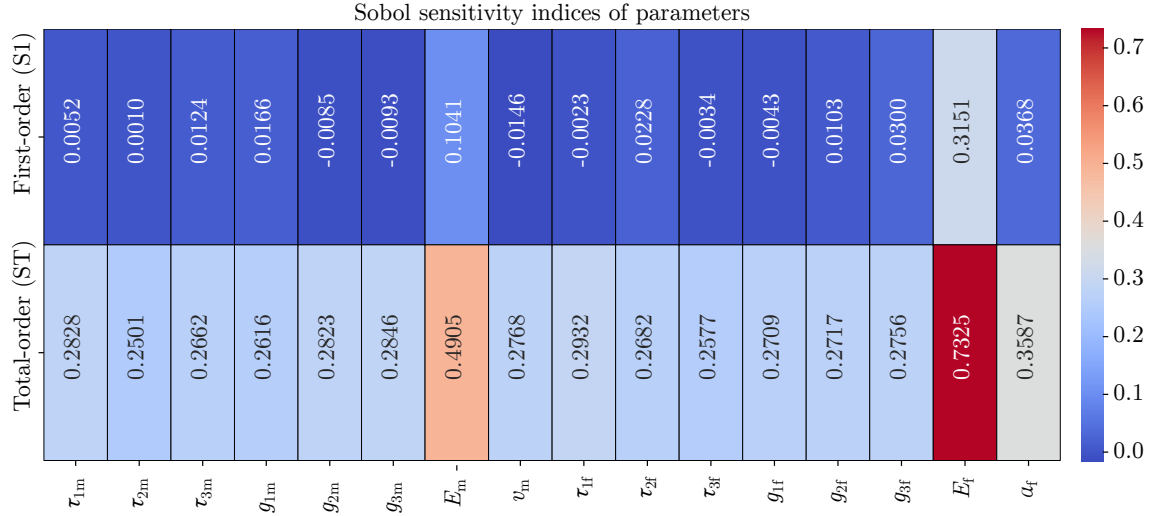


Figure 10: **Sensitivity of the parameters**

library. The reduced component observations corresponding to a specific site were grouped in pairs and represented via ROC curves. A perfect separation between two groups has an area under the curve (AUC) of 1, while an AUC value around 0.5 indicates minimal separation. The results given in Figure 13 suggest that the posterior parameters are not well separated between the distal vs. middle (AUC = 0.50), the middle vs. proximal (AUC = 0.51) and the distal vs. proximal (AUC = 0.51) sites. Furthermore, the kernel density distribution exhibited comparable findings, suggesting a lack of clear separation (Figure 13). Finally, using stochastically inferred parameters from *in-silico* simulations, it is also possible to investigate the stress uncertainties of the fiber and matrix constituents. A typical stress band observed for the distal site is represented in Figure 14, and for middle and proximal results are given in Supplementary Figure S6.

4. Discussion and Conclusions

In-silico simulations using computational techniques have significant potential to model very specific cases, ranging from patient-specific tissue behavior to a large variation in population. One significant factor that influences the outcomes of the simulation is the selected constitutive material model, as well as the parameters used in this model. Homogeneous isotropic hyperelastic materials can capture the biomechanical response of many deformable solids. However, most biological materials exhibit inherent variation in their response and may not be accurately represented by a constitutive model with a single set of deterministic parameters. In this approach, the model is typically verified through forward model evaluations using a certain number of experiments. For the backward problem, an inverse approach is mostly used to identify the input parameters from the output. This method is powerful for the characterization of patient- or specimen-specific materials. To account for the uncertainties in the experimental observations, the standard Bayesian approach is widely implemented in many studies [15, 16, 17, 18, 13]. However, it may not always be possible to derive and express the likelihood function in explicit form, particularly for complex loading scenarios. We suggest a likelihood-free approximate Bayesian computation based on a black-box simulator. We demonstrate its implementation for Achilles tendon specimens from diabetic patients, which include deep uncertainties in their *in-vitro* observations.

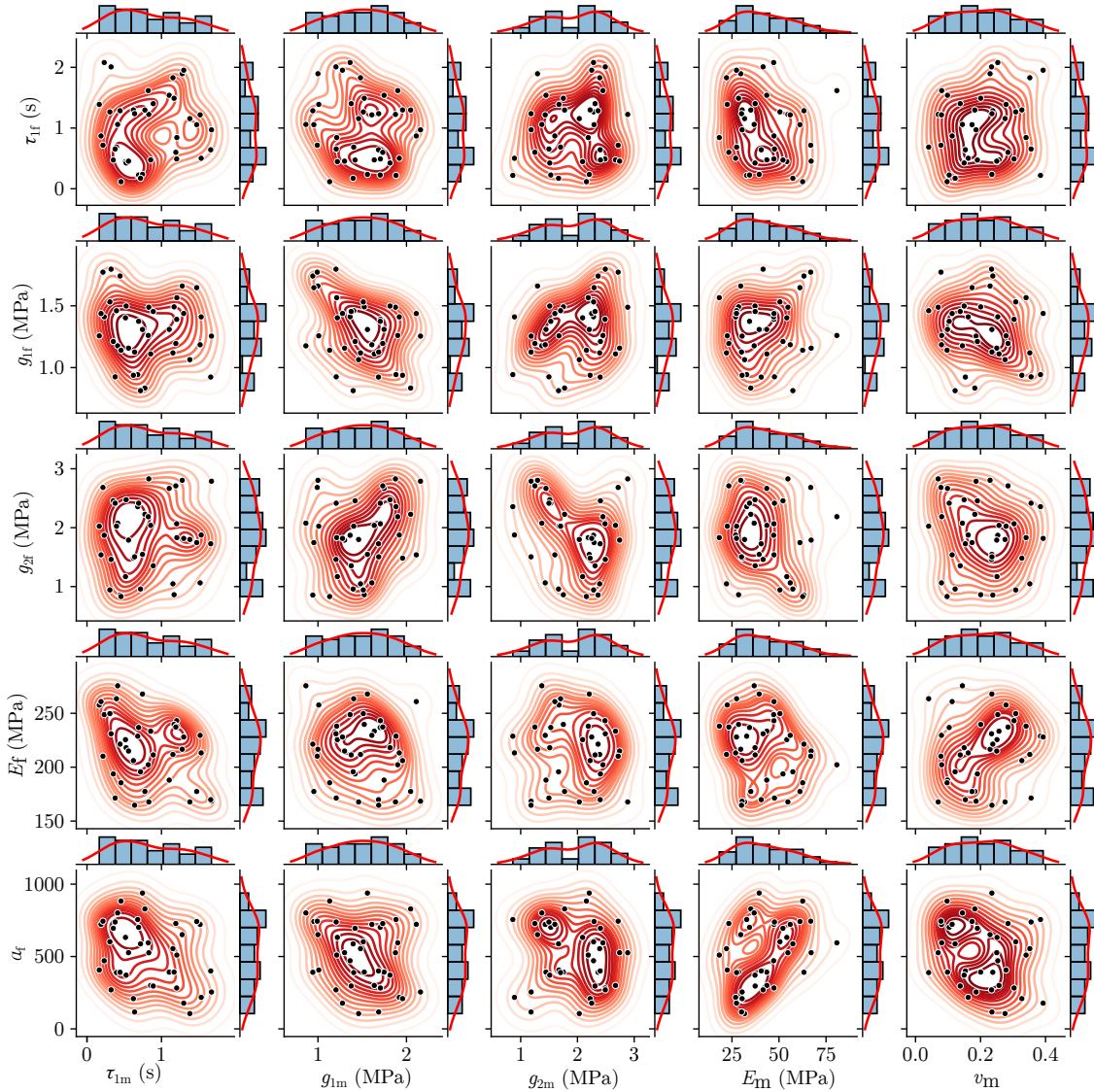


Figure 11: Posterior joint plots between same parameters of the matrix and fiber component for the distal site

472 There are a wide variety of factors, including pathology, microstructural characteristics, tissue
 473 age, and embalming duration, that can significantly influence the biomechanical response. The goal
 474 is to stochastically calibrate parameters that represent the uncertain bounds of experimental obser-
 475 vations without using the likelihood function. We consider the FRVE model for the representation
 476 of *in-vitro* simulations with 16 parameters. **We note that, while the model includes both viscoelas-**
 477 **tic amplitudes and their corresponding relaxation times as free parameters, estimating both sets**
 478 **simultaneously can lead to an ill-posed problem. A common alternative is to fix the relaxation times**
 479 **to a predefined set of values (e.g., 1, 10, 100 s) that span the relevant time scales [49]. This ap-**
 480 **proach reduces parameter dimensionality and computational cost.** We employ ABC-free likelihood
 481 coupled with *in-silico* simulation and *in-vitro* measurement for the estimation of posterior param-
 482 eters. Additionally, Sobol sensitivity analysis and feature importance through a random forest are
 483 performed to investigate the influence of parameters on the model. The overall results we observed
 484 are as follows. First, *in vitro* measurements exhibit extreme uncertainties and variability between

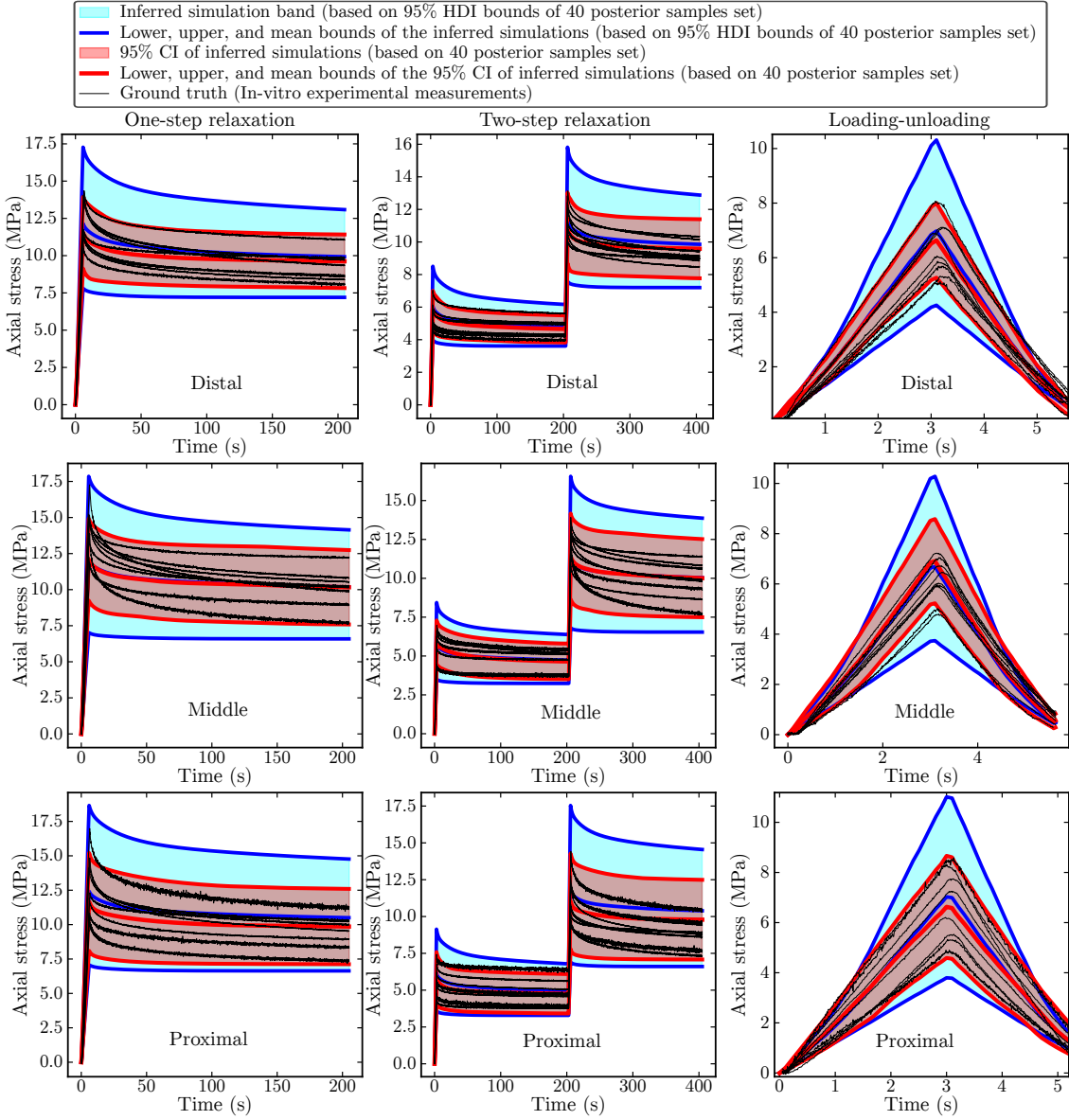


Figure 12: *In-vitro* measurements (ground truth) and inferred simulation observations based on posterior samples for the three sites

samples is high. Second, Bayesian optimization converges rapidly with just a few initial iterations and calibrates 16 specimen-specific parameters. Third, sensitivity analysis and feature importance showed that E_f , α_f , and E_m parameters have the highest influence on the model. Additionally, repeated measures correlation showed a significant correlation between the matrix and fiber viscoelastic parameters. Fourth, the results obtained from ABC demonstrated that the stochastically inferred model parameters can capture the uncertainty band of *in-vitro* measurements (y_{obs}). Fifth, the PCA results demonstrated that the posterior parameters are not separated between sites. For clinical implementation, this observation may suggest that treatment or rehabilitation strategies regarding the mechanical response of diabetic tendons may be generalized to target the entire tendon rather than focusing on specific sites. However, additional data are needed to investigate whether

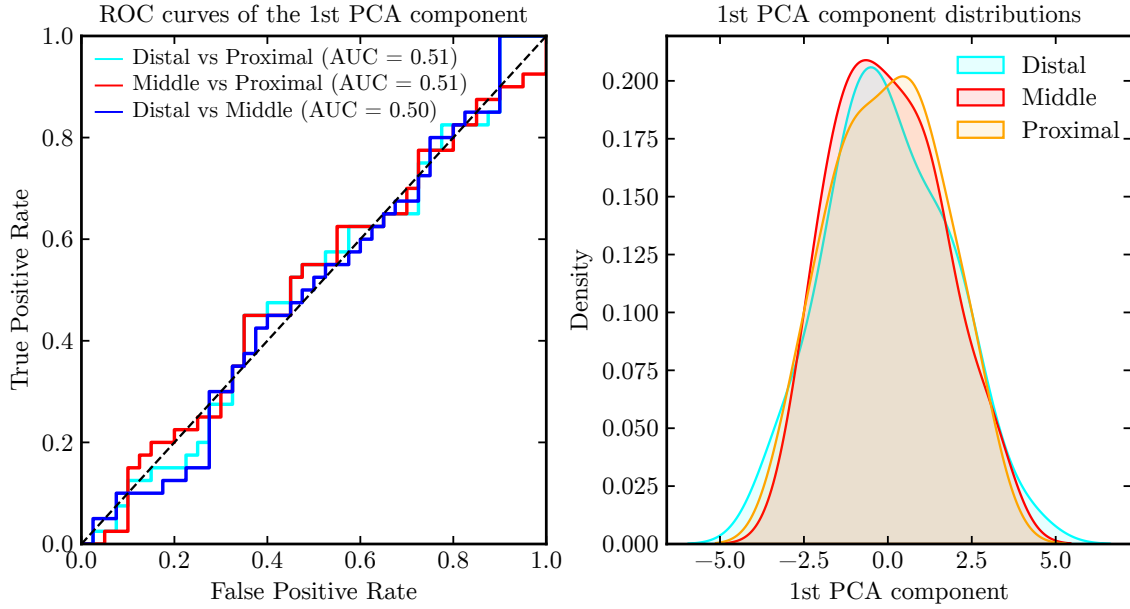


Figure 13: ROC curves and kernel density estimation for the 1st PCA component

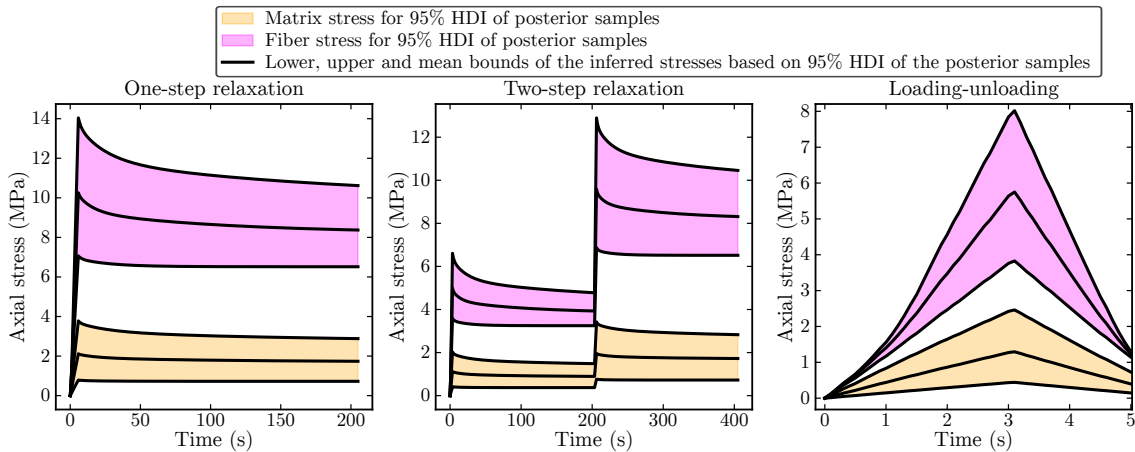


Figure 14: Inferred matrix and fiber stresses for the distal site

495 these findings hold in different patient populations.

496 Although ABC is conceptually simple and can be easily implemented for calibration purposes,
497 it can be computationally expensive due to the high processing time in the simulator. However,
498 we believe that this issue can be addressed by using machine or deep learning algorithms as a
499 surrogate model instead of obtaining y_{sim} observations from the simulator during each step of the
500 ABC sampling update. Once the input parameter set θ_N and the corresponding observations y_{sim}
501 from the forward simulator are trained in the algorithm, unknown simulation observations based on
502 the input parameters sampled in ABC can be predicted using the surrogate model.

503 Mechanical characterization of soft tissue is usually performed by testing n samples and then
504 averaging the model parameters calibrated for n data sets. In some cases, the average of n mea-
505 surements is taken first, and then non-linear curve fitting techniques for the constitutive model are
506 applied to calibrate the parameters for a single data set. In both methods, the calibrated param-

507 eters cannot fully capture the uncertainties in the measurements. Moreover, while uncertainties
508 arising from geometry are often not considered, the proposed method can easily incorporate these
509 uncertainties.

510 This study shows that the parameters calibrated using the probabilistic technique (Table 3) differ
511 from those obtained through the frequentist approach (Table 2). In the frequentist approach, we
512 optimize parameters separately for each specimen based on its own data using Bayesian Optimization
513 (BO). In contrast, in the ABC approach, we use data from all specimens collectively to infer posterior
514 parameter distributions, capturing uncertainty in the estimates. For example, consider the elastic
515 modulus of fiber E_f for the distal site: using the frequentist approach, the average E_f value for nine
516 specimens is 204.82 ± 27.42 MPa (mean \pm standard deviation), whereas the ABC estimate is 216.2
517 ± 31.12 MPa. While this difference illustrates how inference outcomes may vary between methods, it
518 should be interpreted with caution due to key modeling assumptions. For instance, the prior ranges
519 used in the ABC framework were informed by the parameter bounds of BO calibration. Although the
520 observations used in BO and ABC differ, this approach introduces a form of indirect data reuse that
521 may lead to underestimation of posterior uncertainty. Future work should consider using hierarchical
522 ABC models or priors based on external domain knowledge to reduce this potential bias. Similarly,
523 the initial choice of $\epsilon = 0.3$ was made empirically. While the ABC-SMC algorithm adaptively
524 updates this threshold in later generations, the initial value still reflects a modeling decision that
525 may influence the resulting posterior distributions. Furthermore, the following limitations should
526 be addressed in future studies. First, the number of samples is important for the quantification of
527 uncertainty; hence, more specimens should be used to investigate the posterior parameters of the
528 population. Second, investigations are performed on samples with approximately similar geometrical
529 dimensions. Further studies can include geometrical uncertainty. Third, while the concept of ABC
530 is simple and widely applicable, it is computationally expensive as it requires simulating the forward
531 model many times. Additional studies can explore the use of surrogate models based on machine or
532 deep learning algorithms. Finally, this study focused solely on quantifying uncertainty arising from
533 variability in mechanical parameters across specimens with approximately similar geometry. Other
534 important sources of uncertainty—such as measurement noise, model-form errors, and geometric
535 variability—were not considered in the current framework. Future work could extend this approach
536 by incorporating these additional sources of uncertainty.

537 In conclusion, the likelihood-free uncertainty quantification approach provides a useful frame-
538 work for the stochastic calibration of constitutive material model parameters without the need to
539 derive a likelihood function. This general framework can be applied to various combinations of
540 loading data and constitutive models. In medicine, microscale characterization and uncertainty
541 quantification of constituents that cannot be easily determined using experimental techniques, in-
542 cluding constituent parameters, constituent stress, and their correlations, could help create more
543 effective therapeutic strategies.

544 5. Acknowledgments

545 The author greatly thanks Prof. Firat Ozan from Kayseri City Hospital for his constructive
546 comments and suggestions for this work.

Table 2: FRVE model parameters tuned with Bayesian optimization

Site	ID	τ_{1m} (s)	τ_{2m} (s)	τ_{3m} (s)	g_{1m} (MPa)	g_{2m} (MPa)	g_{3m} (MPa)	E_m (MPa)	v_m	τ_{1f} (s)	τ_{2f} (s)	τ_{3f} (s)	g_{1f} (MPa)	g_{2f} (MPa)	g_{3f} (MPa)	E_f (MPa)	α_f	RMSE (N)
Distal	1	0.578	18.626	197.901	1.468	2.100	0.800	59.900	0.240	0.386	17.898	51.569	0.957	1.575	225.145	2.05E3	22.887	
	2	0.407	4.937	60.607	1.315	1.760	1.944	70.000	0.254	1.644	15.729	83.984	0.943	1.629	2.072	206.852	1.09E3	21.352
	3	0.156	14.878	152.518	1.463	0.812	0.981	62.716	0.300	1.549	8.717	20.000	0.905	1.155	0.800	216.049	1.30E3	20.892
	4	1.138	17.810	146.273	1.461	1.715	2.100	31.571	0.240	2.000	20.000	133.023	1.000	2.100	203.115	0.00E0	26.799	
	5	0.819	9.548	194.489	1.352	1.933	0.800	58.204	0.121	2.000	10.558	40.376	0.905	1.245	2.100	244.672	8.62E2	24.957
	6	0.905	18.524	23.824	1.500	1.795	0.800	34.364	0.001	2.000	18.802	169.058	0.821	2.100	2.100	167.979	2.23E2	21.311
	7	2.000	11.041	142.566	1.500	2.100	2.100	70.000	0.400	2.000	20.000	200.000	1.000	2.100	2.100	229.886	0.00E0	14.737
	8	2.000	3.000	113.385	1.472	1.602	2.100	70.000	0.228	2.000	20.000	20.000	0.913	2.100	2.100	182.576	0.00E0	25.667
	9	2.000	20.000	20.000	1.500	2.100	2.100	46.866	0.000	2.000	20.000	200.000	1.000	2.100	2.100	167.365	0.00E0	17.196
Middle	1	2.000	3.000	20.000	0.800	1.678	2.052	63.561	0.400	1.347	20.000	196.344	0.952	1.973	2.100	160.000	0.00E0	21.989
	2	0.921	3.616	153.302	0.800	1.162	2.038	70.000	0.00	0.954	20.000	200.000	0.890	2.100	2.100	195.264	2.86E4	29.958
	3	1.548	6.478	20.000	1.500	0.817	2.100	22.412	0.352	2.000	20.000	164.040	0.912	2.100	2.100	201.470	1.04E4	9.382
	4	2.000	20.000	200.000	1.500	2.100	2.100	70.000	0.400	2.000	20.000	199.514	1.000	2.100	2.100	164.599	0.00E0	41.498
	5	1.970	13.086	69.866	1.168	1.259	2.049	11.000	0.091	1.689	20.000	200.000	0.800	2.100	2.100	199.684	0.00E0	23.908
	6	2.000	3.000	200.000	1.500	2.100	2.100	36.661	0.400	2.000	20.000	200.000	0.986	2.100	2.100	183.405	0.00E0	27.924
	7	2.000	20.000	200.000	1.405	2.100	2.100	45.681	0.400	2.000	20.000	131.544	1.000	2.100	2.100	160.000	0.00E0	36.654
	8	2.000	15.718	200.000	1.500	2.100	2.100	27.279	0.248	1.920	20.000	200.000	1.000	2.100	2.100	183.405	0.00E0	15.228
	9	1.116	16.968	125.238	1.500	0.800	2.096	11.000	0.026	0.789	6.431	113.803	0.800	2.100	2.100	188.961	2.61E2	19.570
Proximal	1	0.651	6.536	45.061	1.473	0.815	2.100	25.626	0.100	1.811	20.000	79.971	0.952	1.819	2.100	271.839	1.47E3	17.278
	2	1.693	12.671	200.000	0.985	1.974	2.100	70.000	0.001	2.000	20.000	200.000	1.000	1.728	2.100	174.056	0.00E0	27.972
	3	2.000	20.000	200.000	1.084	2.100	2.100	70.000	0.094	2.000	20.000	193.850	0.966	2.100	2.100	188.282	0.00E0	41.157
	4	2.000	20.000	200.000	1.500	2.100	2.100	70.000	0.400	2.000	20.000	200.000	0.997	2.100	2.100	236.762	0.00E0	35.313
	5	1.554	20.000	108.220	1.497	2.100	1.675	18.517	0.323	2.000	20.000	145.985	0.953	2.100	2.100	230.546	0.00E0	29.566
	6	1.001	4.105	188.331	1.500	2.100	1.570	70.000	0.305	1.920	20.000	55.307	0.800	1.507	2.100	227.843	4.33E2	20.384
	7	2.000	20.000	200.000	1.500	2.100	2.100	70.000	0.001	2.000	20.000	200.000	1.000	2.100	2.100	275.000	0.00E0	43.663
	8	1.722	5.033	147.013	1.298	1.288	2.043	49.906	0.237	1.693	14.746	85.025	0.974	1.692	1.738	191.018	1.91E3	18.428
	9	1.620	16.161	97.951	0.934	0.849	1.941	11.823	0.001	1.071	18.328	161.805	0.877	2.100	2.100	183.610	0.00E0	16.286

Table 3: Posterior parameters inferred for the three sites

Parameter	Distal	Middle	Proximal
E_f (MPa)	216.2 ± 31.12 (164.6, 267.8)	249.1 ± 46.47 (167.2, 324.9)	238.5 ± 50.04 (161.4, 322.3)
α_f (-)	515.7 ± 224.4 (105.7, 883.0)	566.1 ± 275.9 (76.26, 962.6)	548.9 ± 278.9 (76.26, 962.6)
g_{1f} (MPa)	1.305 ± 0.254 (0.813, 1.772)	1.288 ± 0.280 (0.881, 1.762)	1.252 ± 0.272 (0.881, 1.762)
g_{2f} (MPa)	1.857 ± 0.602 (0.855, 2.828)	1.726 ± 0.676 (0.803, 2.789)	1.814 ± 0.652 (0.803, 2.789)
g_{3f} (MPa)	1.754 ± 0.638 (1.001, 2.896)	1.849 ± 0.629 (0.847, 2.820)	1.741 ± 0.633 (0.847, 2.820)
τ_{1f} (s)	0.988 ± 0.559 (0.116, 2.007)	1.086 ± 0.661 (0.167, 2.077)	1.001 ± 0.623 (0.167, 2.077)
τ_{2f} (s)	11.31 ± 5.395 (2.347, 19.41)	13.06 ± 5.395 (2.798, 21.40)	12.79 ± 5.550 (3.023, 21.75)
τ_{3f} (s)	106.0 ± 49.25 (22.91, 189.5)	120.9 ± 57.21 (30.07, 218.5)	119.9 ± 55.14 (24.44, 218.5)
E_m (MPa)	42.16 ± 14.74 (18.26, 67.07)	46.19 ± 18.76 (14.82, 77.67)	42.76 ± 18.36 (14.82, 79.59)
g_{1m} (MPa)	1.499 ± 0.348 (0.941, 2.158)	1.626 ± 0.440 (0.929, 2.296)	1.600 ± 0.428 (0.929, 2.296)
g_{2m} (MPa)	1.948 ± 0.537 (0.861, 2.742)	1.841 ± 0.600 (1.033, 2.830)	1.752 ± 0.582 (1.012, 2.830)
g_{3m} (MPa)	1.809 ± 0.620 (0.885, 2.834)	1.946 ± 0.528 (1.059, 2.856)	1.898 ± 0.553 (0.896, 2.824)
τ_{1m} (s)	0.814 ± 0.447 (0.188, 1.671)	0.977 ± 0.479 (0.264, 2.042)	0.960 ± 0.531 (0.179, 2.042)
τ_{2m} (s)	12.99 ± 5.199 (3.993, 21.96)	12.12 ± 6.041 (3.521, 22.88)	12.40 ± 6.176 (3.152, 22.15)
τ_{3m} (s)	83.58 ± 46.82 (20.62, 192.6)	112.1 ± 55.61 (24.08, 212.1)	104.8 ± 53.14 (24.08, 212.1)
v_m (-)	0.208 ± 0.095 (0.069, 0.392)	0.202 ± 0.121 (0.015, 0.399)	0.210 ± 0.118 (0.015, 0.399)

The values are represented as mean \pm standard deviation.

The values given in round brackets are the highest density interval (HDI) bounds at 95% level

547 **References**

- 548 [1] M. Viceconti, P. Emili, L.A. E. Courcelles, C. Curreli, N. Famaey, L. Geris, M. Horner, M. C.
549 Jori, A. Kulesza, A. Loewe, M. Neidlin, M. Reiterer, C. F. Rousseau, G. Russo, S. J. Sonntag,
550 E. M. Voisin, F. Pappalardo, Possible Contexts of Use for In Silico Trials Methodologies: A
551 Consensus-Based Review, *IEEE Journal of Biomedical and Health Informatics* 25 (10) (2021)
552 3977–3982. [doi:10.1109/JBHI.2021.3090469](https://doi.org/10.1109/JBHI.2021.3090469).
- 553 [2] T. Smit, N. Aage, D. Haschtmann, S. J. Ferguson, B. Helgason, In silico medical device test-
554 ing of anatomically and mechanically conforming patient-specific spinal fusion cages designed
555 by full-scale topology optimisation, *Frontiers in Bioengineering and Biotechnology* 12 (2024)
556 1347961. [doi:10.3389/fbioe.2024.1347961](https://doi.org/10.3389/fbioe.2024.1347961).
- 557 [3] VV-40, Assessing credibility of computational modeling through verification and validation:
558 Application to medical devices, American Society of Mechanical Engineers (2018).
- 559 [4] M. Pekedis, A. Karaarslan, F. Ozan, T. M., K. C., Novel anchor-type proximal femoral nail for
560 the improvement of bone-fixation integrity in treating intertrochanteric fractures: an exper-
561 imental and computational characterization study, *Computer Methods in Biomechanics and*
562 *Biomedical Engineering* (2025). [doi:10.1080/10255842.2025.2456985](https://doi.org/10.1080/10255842.2025.2456985).
- 563 [5] R. Ogden, G. Saccomandi, I. Sgura, Fitting hyperelastic models to experimental data, *Com-
564 putational Mechanics* 34 (6) (2004) 484–502. [doi:10.1007/s00466-004-0593-y](https://doi.org/10.1007/s00466-004-0593-y).
- 565 [6] M. Pekedis, Uncertainty quantification of hyperelastic soft tissue, in: The 26th Congress of the
566 European Society of Biomechanics, 2021, p. 612.
- 567 [7] S. Budday, T. Ovaert, G. Holzapfel, P. Steinmann, E. Kuhl, Fifty Shades of Brain: A Review
568 on the Mechanical Testing and Modeling of Brain Tissue, *Archives of Computational Methods*
569 in Engineering 27 (4) (2020) 1187–1230. [doi:10.1007/s11831-019-09352-w](https://doi.org/10.1007/s11831-019-09352-w).
- 570 [8] J. Niestrawska, C. Viertler, P. Regitnig, T. U. Cohnert, G. Sommer, G. A. Holzapfel, Mi-
571 crostructure and mechanics of healthy and aneurysmatic abdominal aortas: experimental
572 analysis and modelling, *Journal of the Royal Society Interface* 13 (124) (2016) 20160620.
573 [doi:10.1098/rsif.2016.0620](https://doi.org/10.1098/rsif.2016.0620).
- 574 [9] M. Mengoni, Using inverse finite element analysis to identify spinal tissue behaviour in situ,
575 *Methods* 185 (2021) 105–109. [doi:https://doi.org/10.1016/j.ymeth.2020.02.004](https://doi.org/10.1016/jymeth.2020.02.004).
- 576 [10] B. Narayanan, M. L. Olender, D. Marlevi, E. R. Edelman, F. R. Nezami, An inverse method
577 for mechanical characterization of heterogeneous diseased arteries using intravascular imaging,
578 *Scientific Reports* 11 (1) (2021) 22540. [doi:10.1038/s41598-021-01874-3](https://doi.org/10.1038/s41598-021-01874-3).
- 579 [11] W. Oberkampf, T. Trucano, Hirsch, Verification, validation, and predictive capability in
580 computational engineering and physics, *ASME. Appl. Mech. Rev* 57 (5) (2004) 3–78. [doi:10.1115/1.1767847](https://doi.org/10.1115/1.1767847).
- 582 [12] H. B. Henninger, S. P. Reese, A. E. Anderson, J. A. Weiss, Validation of Computational Models
583 in Biomechanics, *Proceedings of the Institution of Mechanical Engineers. Part H, Journal of*
584 *engineering in medicine* 224 (7) (2010) 801–812. [doi:10.1243/09544119JEIM649](https://doi.org/10.1243/09544119JEIM649).

- 585 [13] L. Mihai, T. Woolley, AS.Goriely, Stochastic isotropic hyperelastic materials: constitutive
586 calibration and model selection, Proc Math Phys Eng Sci 474 (2211) (2018) 20170858.
587 doi:[10.1098/rspa.2017.0858](https://doi.org/10.1098/rspa.2017.0858).
- 588 [14] P. Laz, M. Browne, A review of probabilistic analysis in orthopaedic biomechanics, Proceedings
589 of the Institution of Mechanical Engineers, Part H: Journal of Engineering in Medicine 224 (8)
590 (2010) 927–943. doi:[10.1243/09544119JEIM739](https://doi.org/10.1243/09544119JEIM739).
- 591 [15] S. Madireddy, B. Sista, K. Vemaganti, A Bayesian approach to selecting hyperelastic consti-
592 tutive models of soft tissue, Computer Methods in Applied Mechanics and Engineering 291
593 (2015) 102–122. doi:[10.1016/j.cma.2015.03.012](https://doi.org/10.1016/j.cma.2015.03.012).
- 594 [16] K. Teffera, P. Brewick, A Bayesian model calibration framework to evaluate brain tissue char-
595 acterization experiments, Computer Methods in Applied Mechanics and Engineering 357 (2019)
596 112604. doi:[10.1016/j.cma.2019.112604](https://doi.org/10.1016/j.cma.2019.112604).
- 597 [17] P. Brewick, TK, Uncertainty quantification for constitutive model calibration of brain tissue,
598 Journal of the Mechanical Behavior of Biomedical Materials 85 (2018) 237–255. doi:[10.1016/j.jmbbm.2018.05.037](https://doi.org/10.1016/j.jmbbm.2018.05.037).
- 600 [18] B. Staber, J. Guilleminot, Stochastic hyperelastic constitutive laws and identification proce-
601 dure for soft biological tissues with intrinsic variability, Journal of the Mechanical Behavior of
602 Biomedical Materials 65 (2017) 743–752. doi:[10.1016/j.jmbbm.2016.09.022](https://doi.org/10.1016/j.jmbbm.2016.09.022).
- 603 [19] S. Madireddy, B. Sista, K. Vemaganti, Bayesian calibration of hyperelastic constitutive models
604 of soft tissue, Journal of the Mechanical Behavior of Biomedical Materials 59 (2016) 108–127.
605 doi:<https://doi.org/10.1016/j.jmbbm.2015.10.025>.
- 606 [20] J. Haughton, S. L. Cotter, W. J. Parnell, T. Shearer, Bayesian inference on a microstructural,
607 hyperelastic model of tendon deformation, J. R. Soc. Interface 19 (2022) 1–16. doi:<https://doi.org/10.1098/rsif.2022.0031>.
- 609 [21] J. T. Oden, E. E. Prudencio, A. Hawkins-Daarud, Selection and assessment of phenomenological
610 models of tumor growth, Mathematical Models and Methods in Applied Sciences 23 (07) (2013)
611 1309–1338. doi:[10.1142/S0218202513500103](https://doi.org/10.1142/S0218202513500103).
- 612 [22] J. Chiachio, M. Chiachio, A. Saxena, S. Sankararaman, G. Rus, K. Goebel, Bayesian model
613 selection and parameter estimation for fatigue damage progression models in composites, Inter-
614 national Journal of Fatigue 70 (2015) 361–373. doi:<https://doi.org/10.1016/j.ijfatigue.2014.08.003>.
- 616 [23] H. Rappel, L. Beex, L. Noels, S. Bordas, Identifying elastoplastic parameters with bayes'
617 theorem considering output error, input error and model uncertainty, Probabilistic Engineering
618 Mechanics 55 (2019) 28–41. doi:<https://doi.org/10.1016/j.probengmech.2018.08.004>.
- 619 [24] C. Wang, J. Gao, H. Li, C. Lin, J. L. Beck, Y. Huang, Robust sparse bayesian learning for broad
620 learning with application to high-speed railway track monitoring, Structural Health Monitoring
621 22 (2) (2023) 1256–1272. doi:[10.1177/14759217221104224](https://doi.org/10.1177/14759217221104224).
- 622 [25] Y. Huang, J. L. Beck, H. Li, Multitask sparse bayesian learning with applications in structural
623 health monitoring, Computer-Aided Civil and Infrastructure Engineering 34 (9) (2019) 732–
624 754. doi:<https://doi.org/10.1111/mice.12408>.

- 625 [26] Y. Huang, J. L. Beck, H. Li, Y. Ren, Sequential sparse bayesian learning with applications to
626 system identification for damage assessment and recursive reconstruction of image sequences,
627 Computer Methods in Applied Mechanics and Engineering 373 (2021) 113545. [doi:
628 //doi.org/10.1016/j.cma.2020.113545](https://doi.org/10.1016/j.cma.2020.113545).
- 629 [27] X. Meng, J. L. Beck, Y. Huang, H. Li, Adaptive meta-learning stochastic gradient hamiltonian
630 monte carlo simulation for bayesian updating of structural dynamic models, Computer Methods
631 in Applied Mechanics and Engineering 437 (2025) 117753. [doi:
https://doi.org/10.1016/j.cma.2025.117753](https://doi.org/10.1016/j.
632 cma.2025.117753).
- 633 [28] I. Babuška, Z. Sawlan, M. Scavino, B. Szabó, R. Tempone, Bayesian inference and model
634 comparison for metallic fatigue data, Computer Methods in Applied Mechanics and Engineering
635 304 (2016) 171–196. [doi:
https://doi.org/10.1016/j.cma.2016.02.013](https://doi.org/10.1016/j.cma.2016.02.013).
- 636 [29] S. Xue, W. Zhou, J. L. Beck, Y. Huang, H. Li, Damage localization and robust diagnostics in
637 guided-wave testing using multitask complex hierarchical sparse bayesian learning, Mechanical
638 Systems and Signal Processing 197 (2023) 110365. [doi:
https://doi.org/10.1016/j.ymssp.2023.110365](https://doi.org/10.1016/j.ymssp.
639 2023.110365).
- 640 [30] T. Toni, M. Stumpf, Simulation-based model selection for dynamical systems in systems and
641 population biology, Bioinformatics 26 (1) (2010) 104–110. [doi:
10.1093/bioinformatics/btp619](https://doi.org/10.1093/bioinformatics/
642 btp619).
- 643 [31] Y. Schälte, E. Klinger, E. Alamoudi, J. Hasenauer, pyabc: Efficient and robust easy-to-use
644 approximate bayesian computation, Journal of Open Source Software 7 (74) (2022) 4304. [doi:
10.21105/joss.04304](https://doi.org/10.21105/joss.04304).
- 646 [32] G. Qian, Z. Wu, Z. Hu, M. Todd, Pitting corrosion diagnostics and prognostics for miter gates
647 using multiscale simulation and image inspection data, Structural Health Monitoring 0 (0)
648 (2025) 14759217241264291. [doi:
10.1177/14759217241264291](https://doi.org/10.1177/14759217241264291).
- 649 [33] H. Jin, W. Du, G. Yin, Approximate bayesian computation design for phase i clinical tri-
650 als, Statistical Methods in Medical Research 31 (12) (2022) 2310–2322. [doi:
10.1177/09622802221122402](https://doi.org/10.1177/
651 09622802221122402).
- 652 [34] G. Iyengar, R. Singal, Model-free approximate bayesian learning for large-scale conversion
653 funnel optimization, Production and Operations Management 33 (3) (2024) 775–794. [doi:
10.1177/10591478241231857](https://doi.org/10.1177/10591478241231857).
- 655 [35] M. Pekedis, F. Ozan, M. Melez, Location-dependent biomechanical characterization of the hu-
656 man achilles tendon in diabetic and nondiabetic patients, Journal of Biomechanical Engineering
657 (2025). [doi:
10.1115/1.4068015](https://doi.org/10.1115/1.4068015).
- 658 [36] S. A. Maas, B. J. Ellis, G. A. Ateshian, J. A. Weiss, FEBio: Finite Elements for Biomechanics,
659 Journal of Biomechanical Engineering 134 (1) (2012) 011005. [doi:
10.1115/1.4005694](https://doi.org/10.1115/1.4005694).
- 660 [37] J. A. Weiss, B. N. Maker, S. Govindjee, Finite element implementation of incompressible,
661 transversely isotropic hyperelasticity, Computer Methods in Applied Mechanics and Engineer-
662 ing 135 (1) (1996) 107–128. [doi:
https://doi.org/10.1016/0045-7825\(96\)01035-3](https://doi.org/10.1016/0045-7825(96)01035-3).
- 663 [38] P. I. Frazier, A tutorial on bayesian optimization (2018). [arXiv:1807.02811](https://arxiv.org/abs/1807.02811), [doi:
10.48550/arXiv.1807.02811](https://doi.org/10.48550/arXiv.1807.02811).

- 665 [39] P. Dutov, O. Antipova, S. Varma, J. P. R. O. Orgel, J. D. Schieber, Measurement of Elastic
666 Modulus of Collagen Type I Single Fiber, PLoS ONE 11 (2016) e0145711. [doi:10.1371/journal.pone.0145711](https://doi.org/10.1371/journal.pone.0145711).
- 668 [40] H. Khayyeri, A. Gustafsson, A. Heijerjans, M. K. Matikainen, P. Julkunen, P. Eliasson,
669 P. Aspenberg, H. Isaksson, A Fibre-Reinforced Poroviscoelastic Model Accurately Describes
670 the Biomechanical Behaviour of the Rat Achilles Tendon, PLOS ONE 10 (6) (2015) e0126869.
671 [doi:10.1371/journal.pone.0126869](https://doi.org/10.1371/journal.pone.0126869).
- 672 [41] G. Lewis, K. M. Shaw, Modeling the tensile behavior of human Achilles tendon, Bio-Medical
673 Materials and Engineering 7 (4) (1997) 231–244.
- 674 [42] L. Breiman, J. Friedman, R. Olshen, C. Stone, Classification and Regression Trees, Chapman
675 and Hall/CRC, e-book:2017. [doi:10.1201/9781315139470](https://doi.org/10.1201/9781315139470).
- 676 [43] J. Herman, W. Usher, SALib: An open-source Python library for Sensitivity Analysis, The
677 Journal of Open Source Software 2 (9) (2017) 97. [doi:10.21105/joss.00097](https://doi.org/10.21105/joss.00097).
- 678 [44] A. Saltelli, M. Ratto, T. Andres, F. Campolongo, J. Cariboni, D. Gatelli, M. Saisana,
679 S. Tarantola, [Global Sensitivity Analysis: The Primer](#), John Wiley & Sons, 2008.
680 URL <https://www.wiley.com/en-us/Global+Sensitivity+Analysis%3A+The+Primer-p-9780470059975>
- 682 [45] B. Iooss, P. Lemaître, A review on global sensitivity analysis methods, in: G. Dellino, C. Meloni
683 (Eds.), Uncertainty Management in Simulation-Optimization of Complex Systems, Vol. 59 of
684 Operations Research/Computer Science Interfaces Series, Springer, 2015, pp. 101–122. [doi:10.1007/978-1-4899-7547-8_5](https://doi.org/10.1007/978-1-4899-7547-8_5).
- 686 [46] A. Saltelli, P. Annoni, I. Azzini, F. Campolongo, M. Ratto, S. Tarantola, Variance based
687 sensitivity analysis of model output. design and estimator for the total sensitivity index, Com-
688 puter Physics Communications 181 (2) (2010) 259–270. [doi:<https://doi.org/10.1016/j.cpc.2009.09.018>](https://doi.org/10.1016/j.cpc.2009.09.018).
- 690 [47] A. L. L. F. Price, C. C. Drovandi, D. J. Nott, Bayesian synthetic likelihood, Journal of Compu-
691 tational and Graphical Statistics 27 (1) (2018) 1–11. [doi:10.1080/10618600.2017.1302882](https://doi.org/10.1080/10618600.2017.1302882).
- 692 [48] R. Wilkinson, Approximate bayesian computation (abc) gives exact results under the assump-
693 tion of model error (2013). [doi:10.1515/sagmb-2013-0010](https://doi.org/10.1515/sagmb-2013-0010).
- 694 [49] M. Jirásek, P. Havlásek, Accurate approximations of concrete creep compliance functions based
695 on continuous retardation spectra, Computers & Structures 135 (2014) 155–168. [doi:<https://doi.org/10.1016/j.compstruc.2014.01.024>](https://doi.org/10.1016/j.compstruc.2014.01.024).